Numerical Modeling of Flow Control with Electrical Discharges

Integrity ★ Service ★ Excellence

November 2014

Dr. Jonathan Poggie
Senior Aerospace Engineer
Air Force Research Laboratory

High-Speed Flow Research Group

- AFRL/RQ Computational Sciences Center
- Collaboration with experimental groups
- Plasma flow control since late 1990s
- Interesting challenges
  - Applications
  - Plasma physics, chemistry, fluid dynamics
  - Resolution of disparate scales
  - Computational techniques
  - Very large, multidisciplinary simulations

Reentry MHD

MHD Generator Configurations

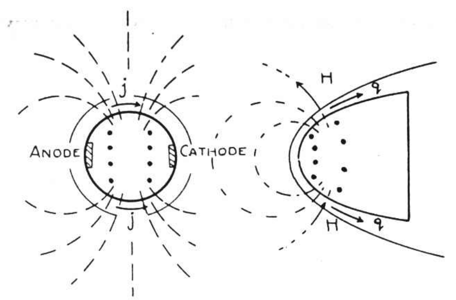

Resler & Sears (1958)

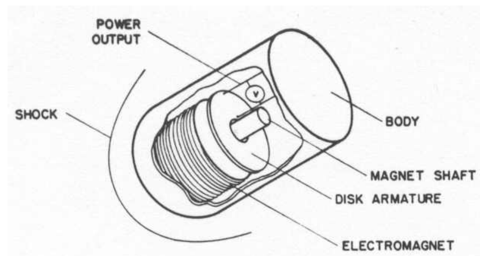

Kranc, Porter & Cambel (1967)

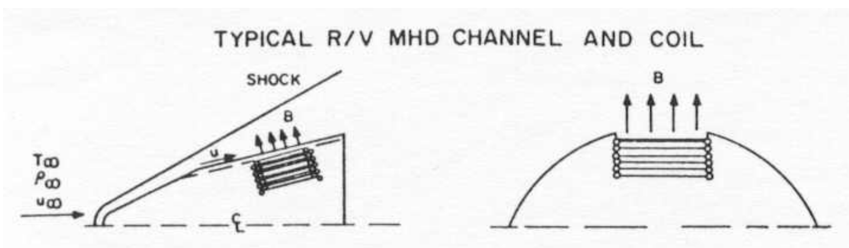

Donaldson & Brunner (1964)

Kantrowitz (1955): If reentry flows are going to be ionized, why not try to control them using electromagnetic effects?

Stagnation Point Heat Transfer Mitigation

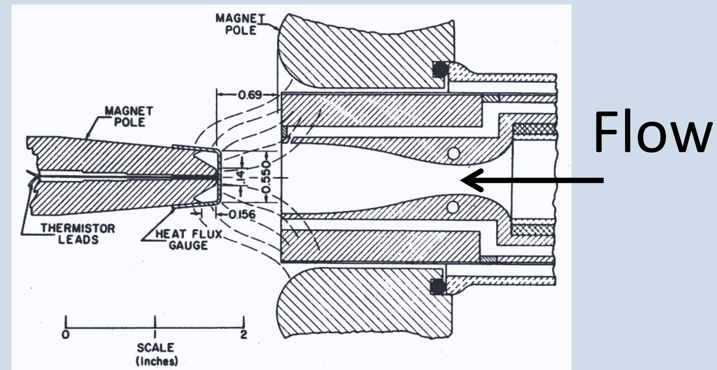

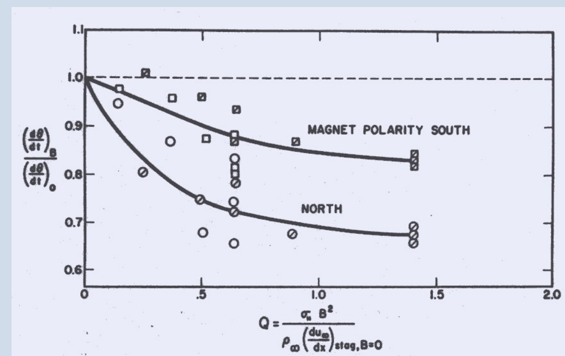

Mach 3 argon flow
Wilkinson (1964)

AYAKS (AJAX) Hypersonic Vehicle Concept

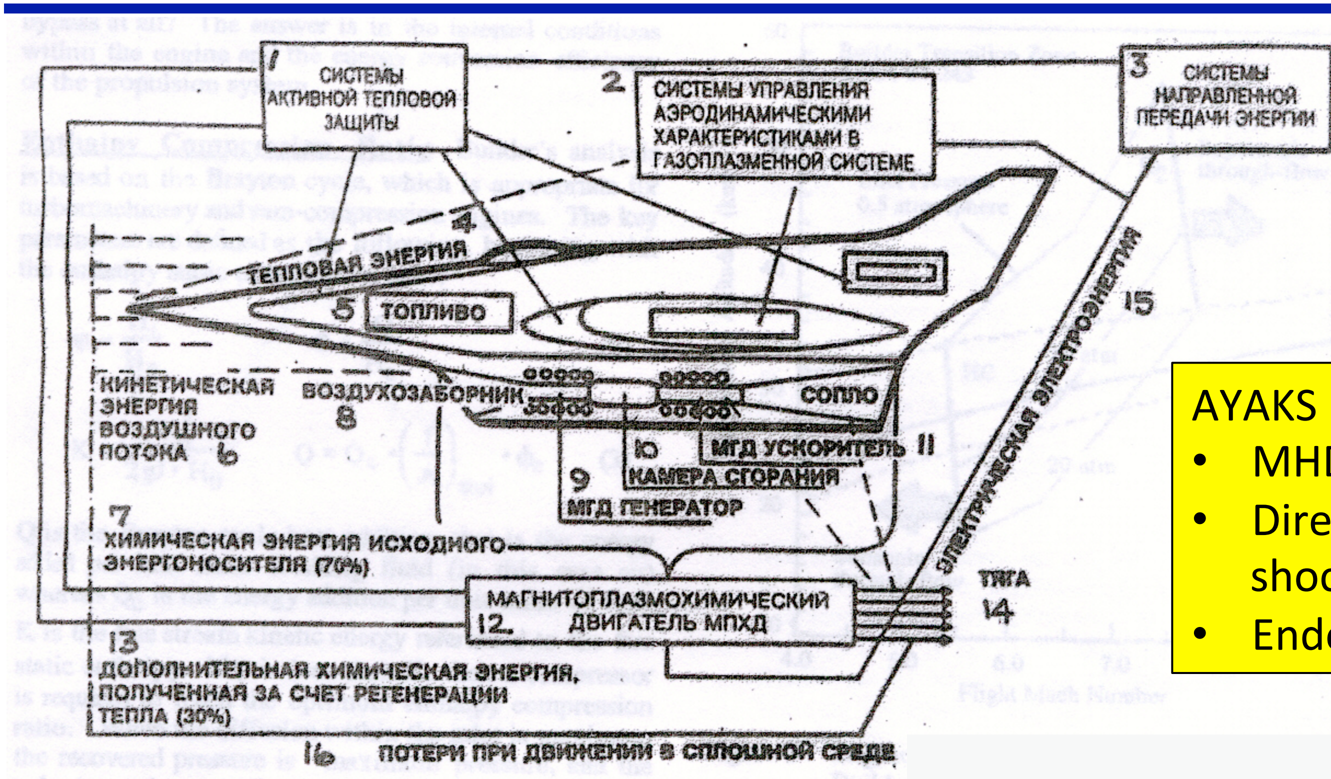

Military Parade Magazine, May/June 1994

AYAKS Features

- MHD energy bypass in engine
- Directed energy beam for bow shock control
- Endothermic fuels

- Design developed in Soviet Union in 1980s under Vladimir Fraishtadt, Leninetz Co.
- Weight tradeoff

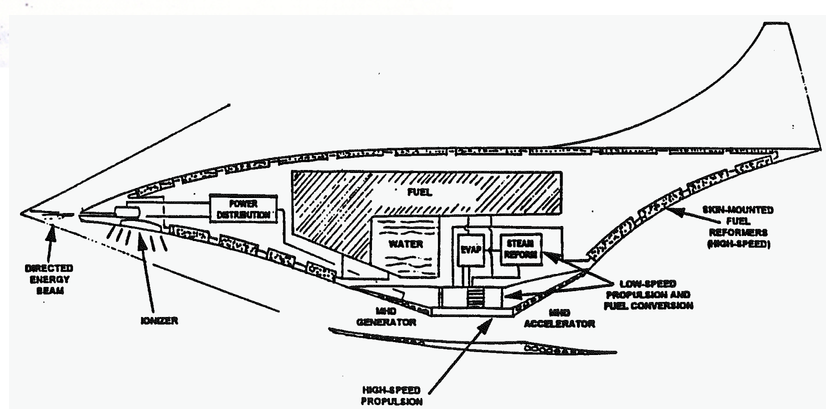

AIAA Paper 1996-4609

Plasma Actuators

Corona Discharge
for Drag Reduction

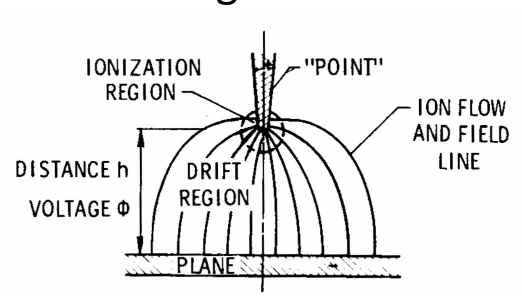

(b) STREAM FUNCTION

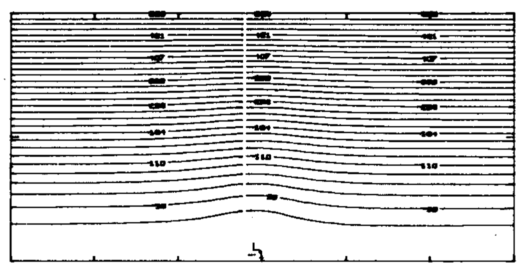

(a) VORTICITY

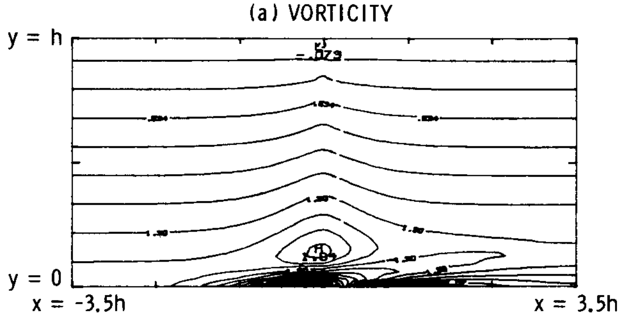

Malik et al., AIAA Paper 1983-0231

ns-DBD Actuators

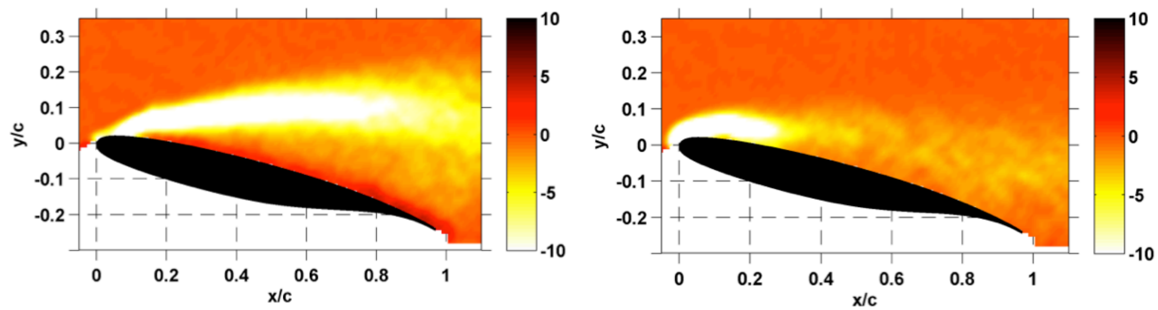

Freestream speed 60 m/s
Little et al. AIAA J., 2012

Actuators produce greatest benefit where they can drive a flow instability

Plasma Aerodynamics: Current Status of Field

- Long history: where are we now?
- AIAA Plasma Aerodynamics Discussion Group
  - Plasma-based flow control
  - Plasma-enhanced combustion
- White paper, http://www.aiaa.org/PlasmaAeroWhitePaper_June2014/
- Aerospace America, November 2014, http://www.aerospaceamerica.org/Pages/Archives.aspx

Higher-Order Plasma Solver

Thermochemical Nonequilibrium

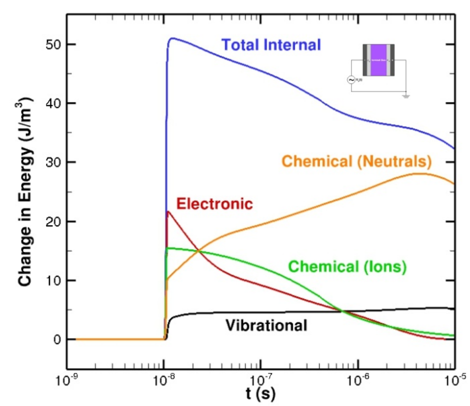

Viscous Flow

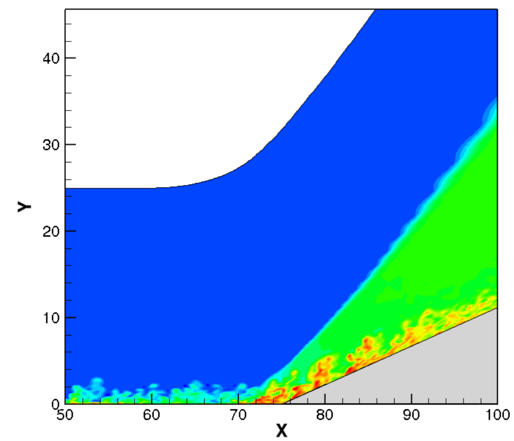

Electrical Discharges

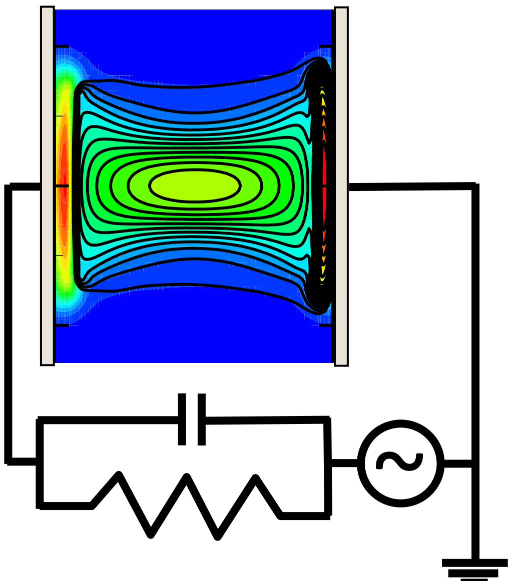

Maxwell's Equations

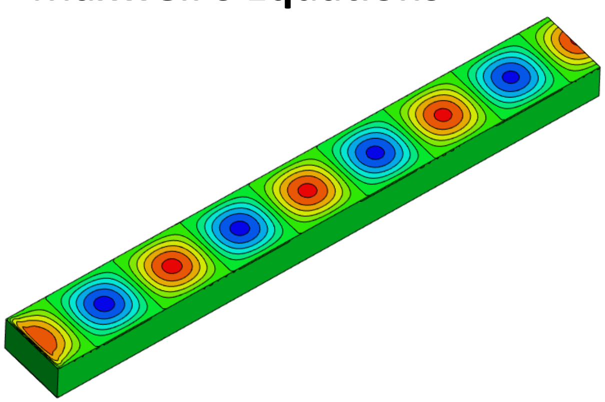

High-order numerics implemented in a multi-fluid context

Acknowledgements

- Funding
  - AFRL In-House Applied Research Funding
  - AFOSR: J. Schmisseur / I. Leyva, Aerothermodynamics
  - AFOSR: F. Fahroo, Computational Mathematics
- DoD HPCMP Computer Time
  - Frontier Project (90M cpu-hr/FY14)
  - AFRL (17M cpu-hr/FY14)
- Codes: G. Candler (US3D), M. Visbal (FDL3DI), I. Boyd (LeMANS)
- Organization
  - Computational Sciences Center: J. Benek
  - High-Speed Systems Division: T. Jackson, R. Kimmel
  - High-Speed Flow Research Group: N. Bisek, R. Gosse, T. Leger
- Helpful discussions: D. Gaitonde, A. Smits, I. Adamovich, I. Boyd, many others

DoD HPCMP Frontier Project

Year	CPU-Hrs (millions)
2014	90
2015	150
2016	211
2017	890
2018	890

Title: Unsteady Pressure and Heating Environment on High-Speed Vehicles with Responding Structures
PI: Dr. Ryan Gosse, AFRL/RQHV

DoD supercomputer resources address stiff, multi-disciplinary physics

Garnet / ERDC: 150k cores

Top 500 List (July 2014)
24. Spirit
31. Garnet
114. Pershing

Scaling to 10^5 Cores

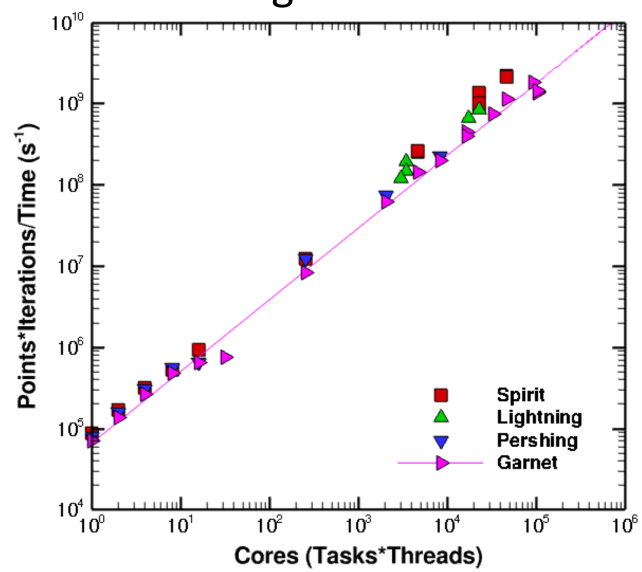

http://www.top500.org

Outline

1. Reentry MHD
2. Plasma actuators
3. Control of separation unsteadiness
4. Turbulence

Reentry Magnetohydrodynamics

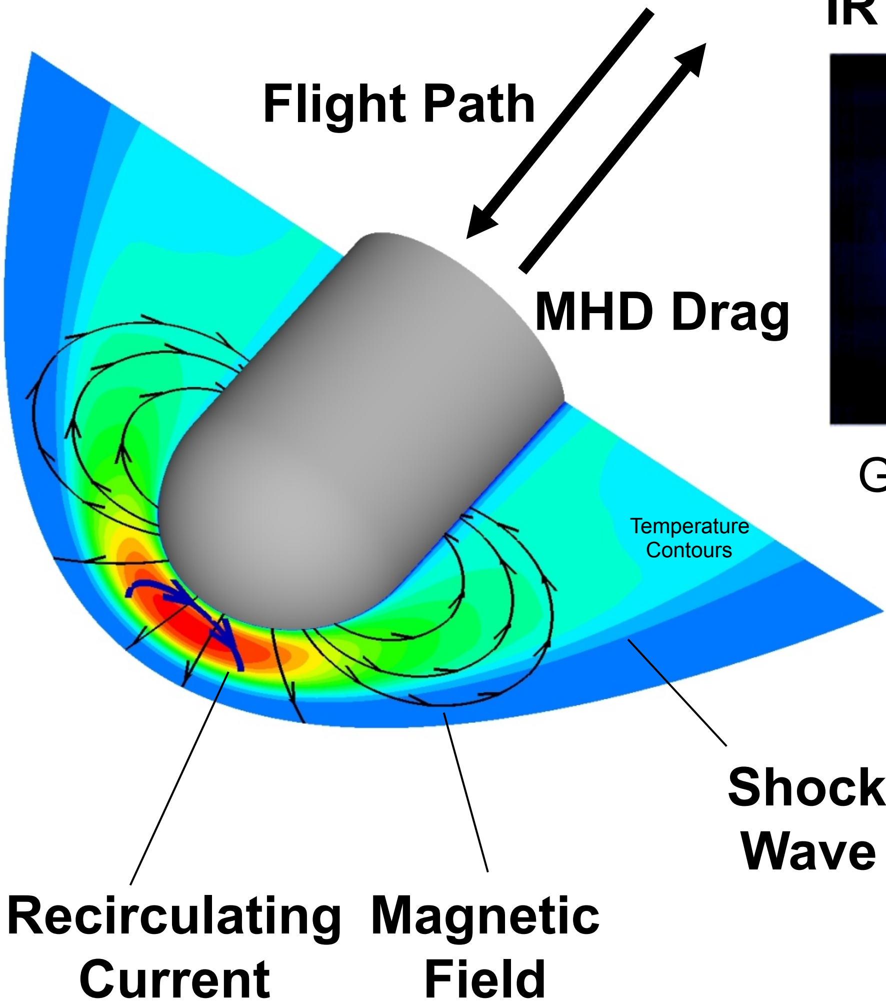

IR Photographs Show Reduced Heating

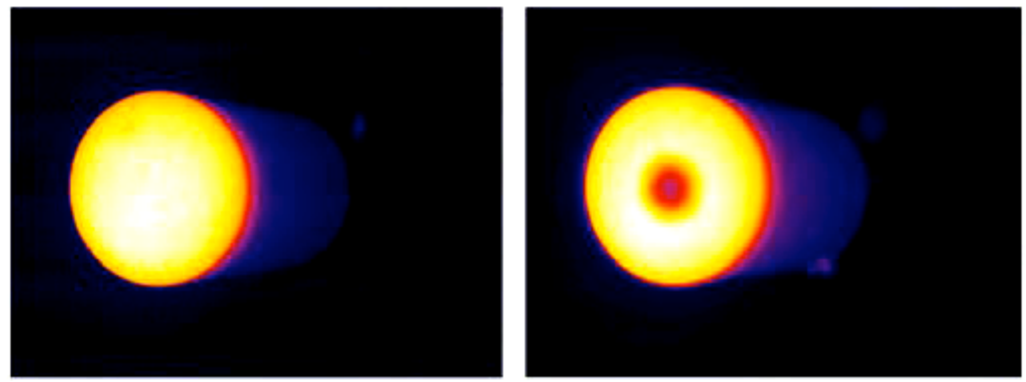

Gülhan et al., J. Spacecraft & Rockets (2009)

Magnetic Force
- Decelerates flow
- Slows vehicle
- Reduces reentry heating

Physical Model

Conservation Equations

$$\frac{\partial \rho_s}{\partial t} + \nabla \cdot (\rho_s \mathbf{u} + J_s) = \dot{w}_s$$

$$\frac{\partial \rho \mathbf{u}}{\partial t} + \nabla \cdot (\rho \mathbf{u}\mathbf{u} - \tau) + \nabla p = \mathbf{j} \times \mathbf{B}$$

$$\frac{\partial E}{\partial t} + \nabla \cdot ((E + p)\mathbf{u} - \tau \cdot \mathbf{u} + \mathbf{q} + \Sigma(J_s\, h_s)) = \mathbf{j} \cdot \mathbf{E}$$

$$\frac{\partial E_{ve}}{\partial t} + \nabla \cdot ((E_{ve})\mathbf{u} + q_{ve} + \Sigma(J_s\, e_{v,s})) = \dot{w}_{ve} + \gamma(\mathbf{E} + \mathbf{u} \times \mathbf{B}) \cdot \mathbf{j}$$

Model Features

- Nonequilibrium ionization
- Low magnetic Reynolds number
- Hall effect and ion slip

Ohm's Law

$$\nabla \cdot \tilde{\sigma} \cdot [-\nabla\phi + \mathbf{u} \times \mathbf{B}] = 0$$

$$\mathbf{E} = -\nabla\phi \qquad \mathbf{j} = \tilde{\sigma} \cdot (\mathbf{E} + \mathbf{u} \times \mathbf{B})$$

MHD Heat Shield

Change in Shock Standoff Distance

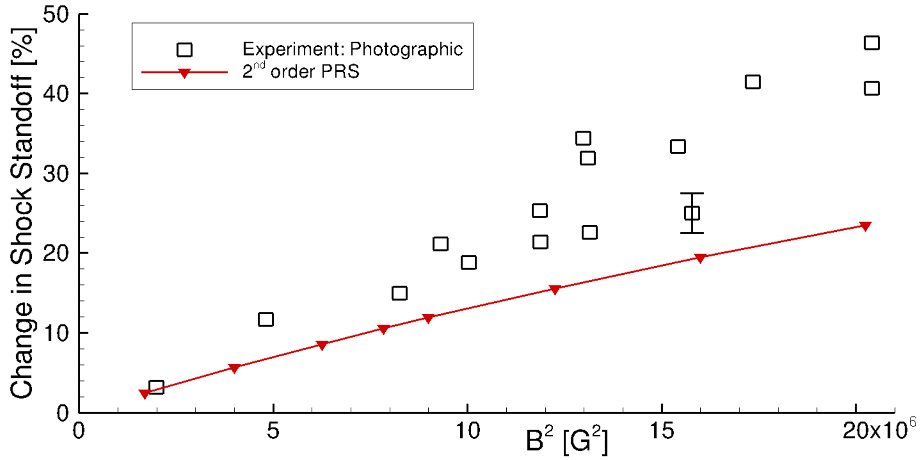

Experiment: Argon flow at Mach 4.75 (Kranc et al., 1969)

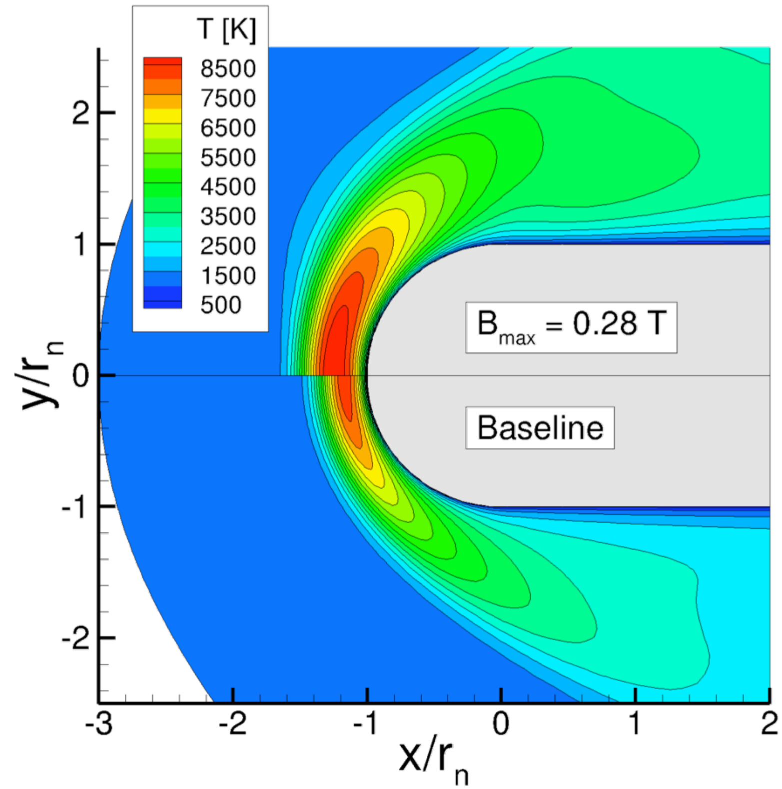

10% reduction in peak heating
Hall effect neglected

N. J. Bisek, I. D. Boyd, and J. Poggie, Journal of Spacecraft and Rockets, 2010

Hall Effect

Hall Effect Neglected

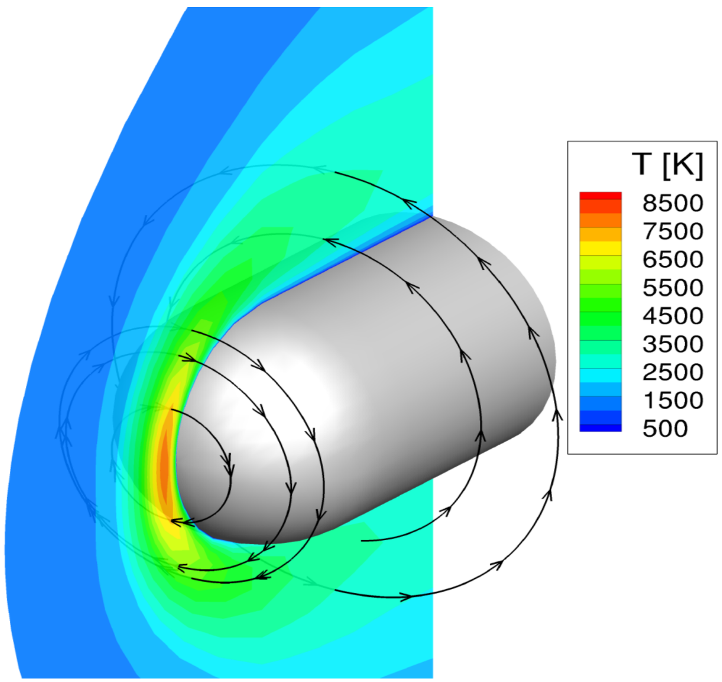

With Hall Effect

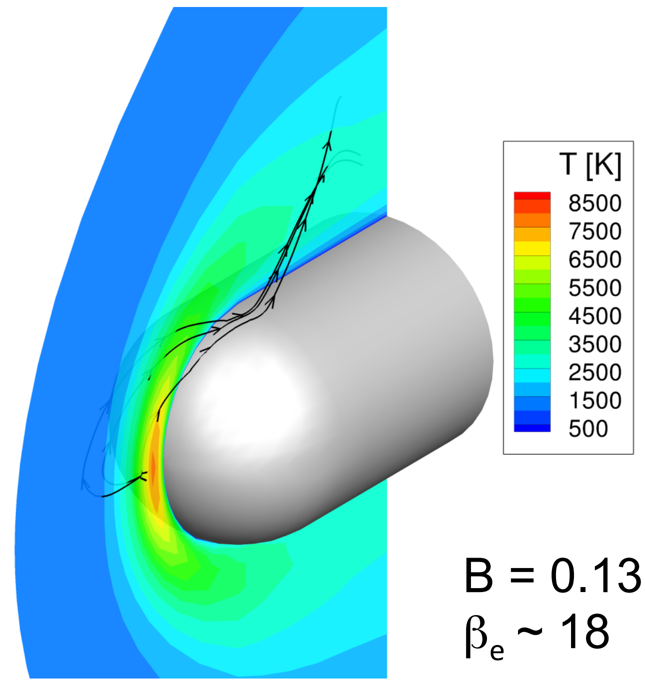

B = 0.13 T

$\beta_e \sim 18$

$$\beta_e = \mu_e B = \sigma B/(e\, n_e)$$

- Large Hall parameter for this experiment
- Hall effect inhibits effect of control

Nanosecond-Pulse DBD Experiments

Pulsed Heating Model Predicts Shock Speed

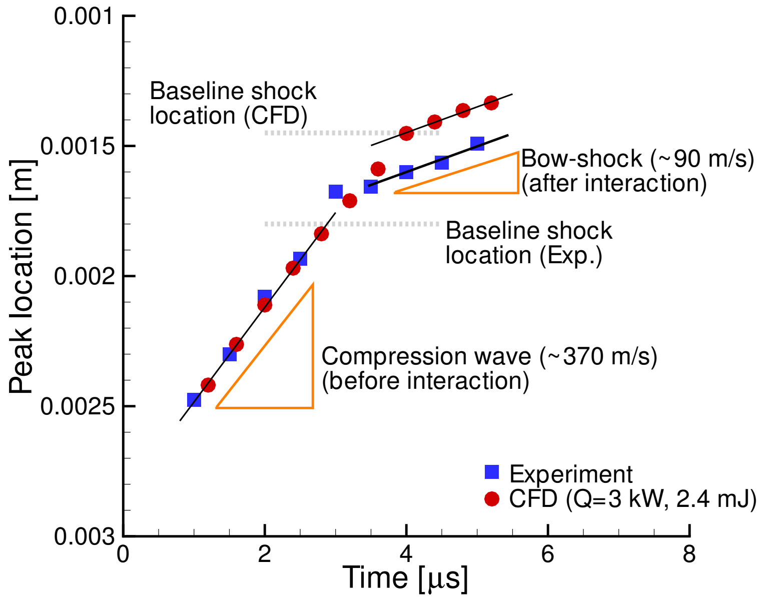

N. Bisek, J. Poggie, M. Nishihara, and I. Adamovich, Journal of Thermophysics and Heat Transfer, 2014.

Phase-Locked Schlieren Images

OSU NETL Mach 5 Wind Tunnel

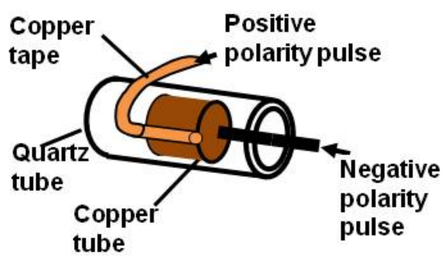

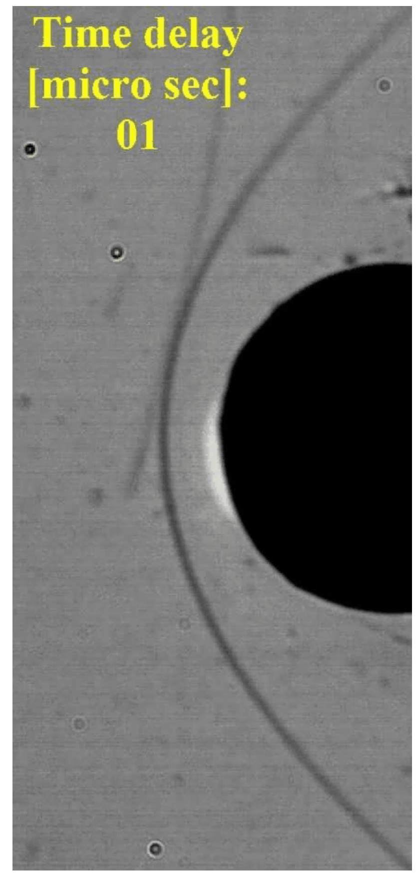

ns-DBD Model

Discharge Configuration

Cylinder Flow Stagnation Conditions

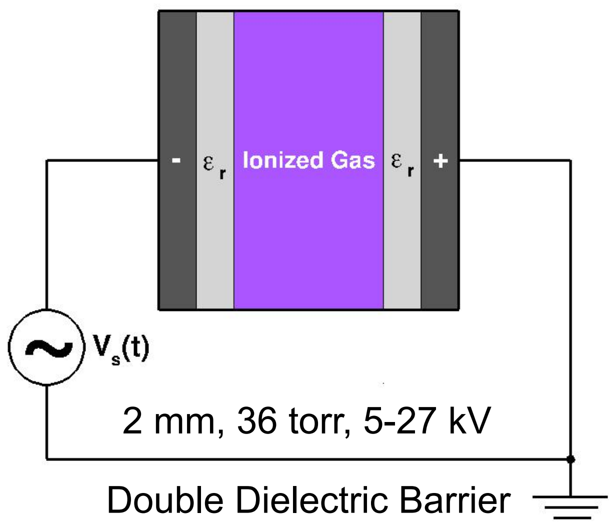

Governing Equations

- Overall mass-averaged conservation laws
- Neutrals: diffusion equation
- Charged particles: mass, momentum, and energy conservation equations
- Poisson equation

Rates: function of electron temperature

J. Poggie, I. Adamovich, N. Bisek, and M. Nishihara, Plasma Sources Science and Technology, 2013.

Air Plasma Kinetic Model

- 23 species, 50 processes
- Ground-state neutrals: N_2, O_2, O, N, NO, O_3
- Charged particles: e^-, N_2^+, O_2^+, O^+
- Electronically excited states: $N_2(A^3\Sigma)$, $N_2(B^3\Pi)$, $N_2(a'^1\Sigma)$, $N_2(C^3\Pi)$, $O(^1D)$
- Vibrationally excited states: $N_2(v=1\text{-}8)$

Discharge Profiles

Number Density and Electric Field

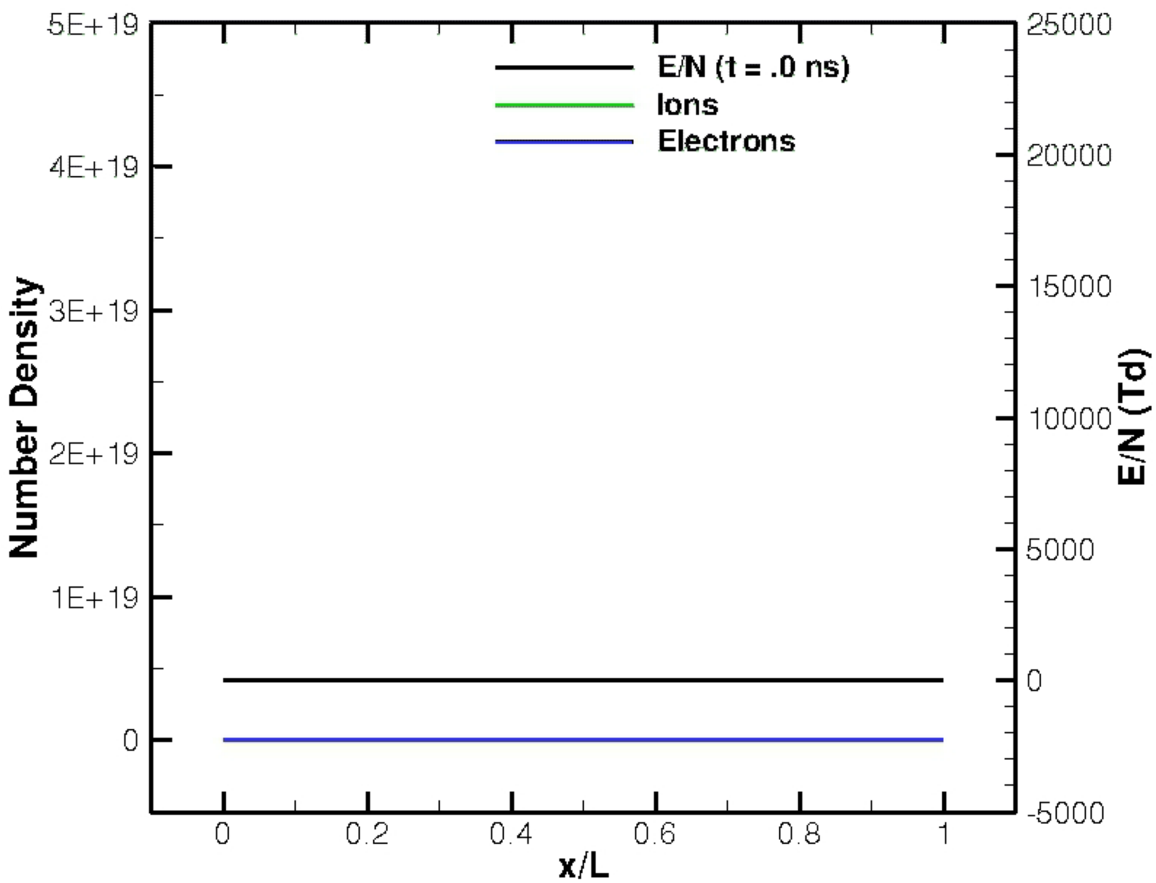

- Breakdown
- Left sheath formation
- Right sheath formation
- Recombination over longer time scale

$V_0 = 27$ kV

Next: once quasi-neutral, switch to larger time step

Wave Motion

Bulk Gas Velocity Profiles

$V_0 = 27$ kV

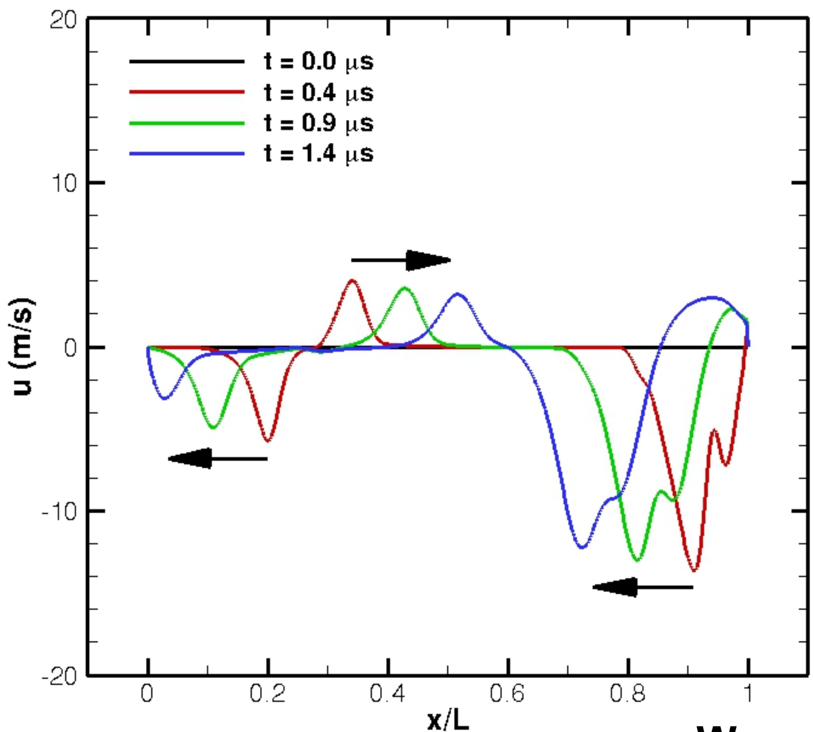

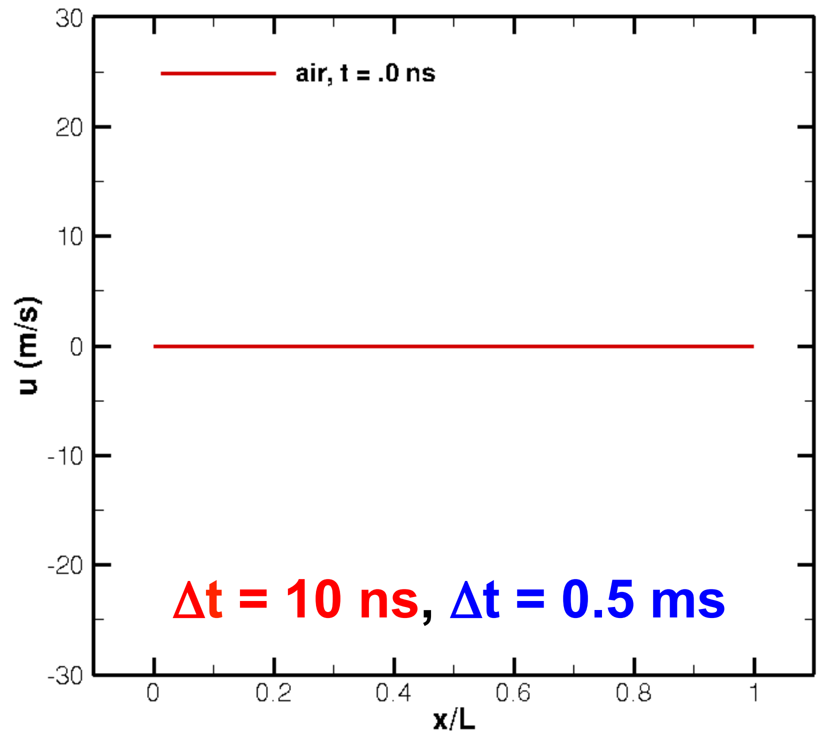

Wave Speed
Measured: 375 m/s
Computed: 340-380 m/s

2D ns-DBD Simulations

Electron Number Density

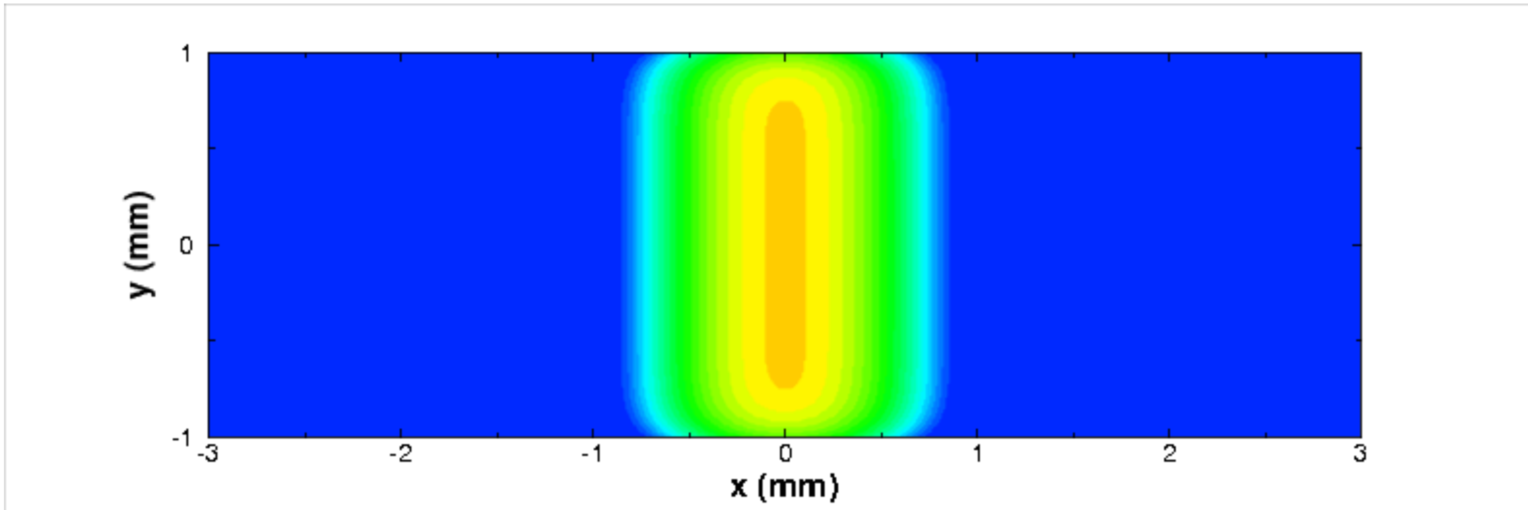

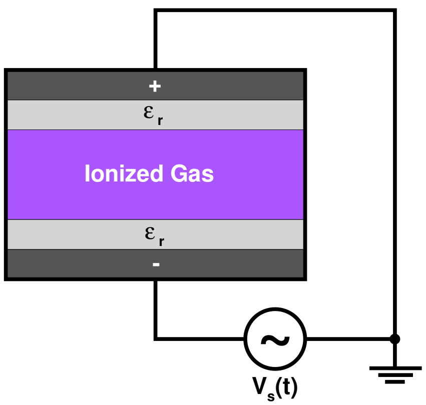

36 torr
2mm gap
2 kV

Next step: compute wave motion due to rapid gas heating

Closed-Loop Stall Control Experiment

- **Participants**
  - **J. Poggie, C. Tilmann, P. Flick - *Air Force Research Laboratory***
  - **J. Silkey, B. Osborne - *The Boeing Company***
  - **G. Ervin, D. Maric - *FlexSys, Inc***
  - **S. Mangalam, A. Mangalam - *Tao Systems, Inc***
- **Demonstrate closed-loop stall sense and control system for subsonic aircraft**
- **Integrate three technologies**
  - **Morphing structures (FlexSys)**
  - **Instantaneous flow topology sensing (Tao Systems)**
  - **DBD plasma actuators (Boeing Co.)**
- **Example of an AFRL technology demonstration program**

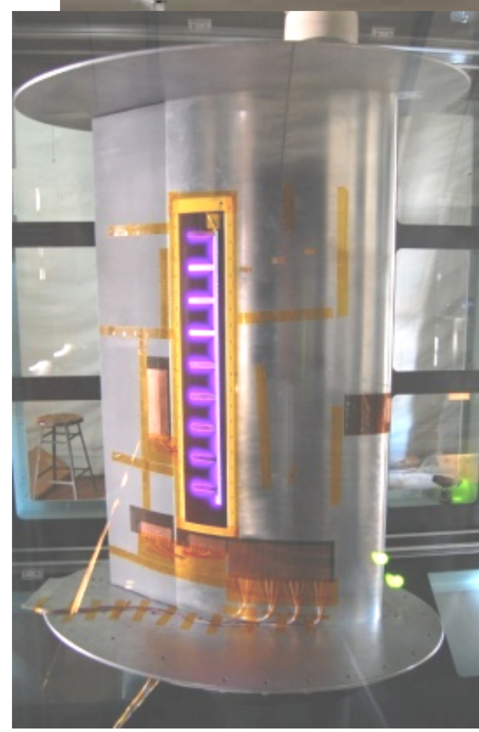

FlexSys, Inc.

Wind Tunnel Installation

AFRL SARL Wind Tunnel Facility

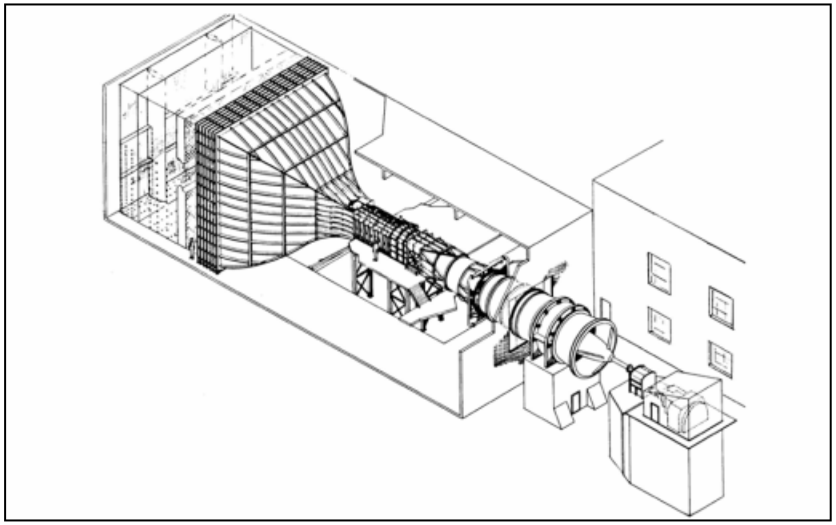

Upstream View

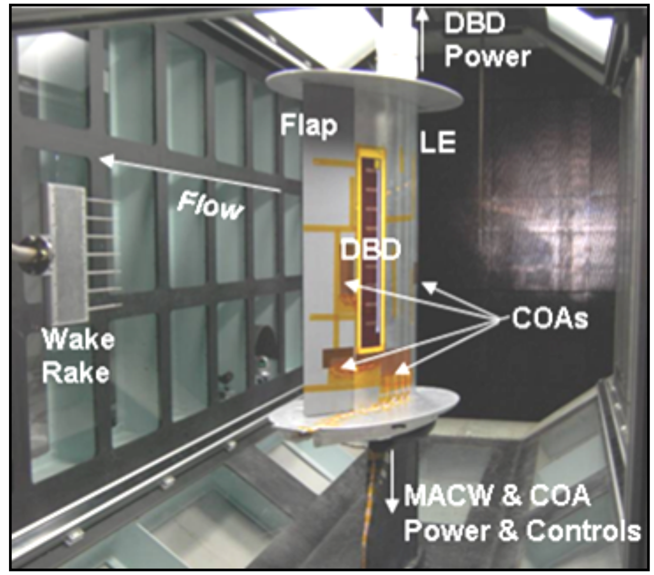

Mach 0.05-0.5
Test Section: 63.1 ft^2, 15 ft long
(5.86 m^2, 4.57 m)

Airfoil: 50 in span x 30 in chord
(1.27 m x 0.76 m)
Elliptical endplates: 45 in x 24 in
(1.14 m x 0.61 m)
Mach number: 0.05-0.10
Reynolds number: $0.9x10^6$ -$1.7x10^6$
AoA: up to 22 deg, Flap: +/- 10 deg
Turbulent boundary layer state

Poggie et al., J. Aircraft, 2010

Closed-Loop Control

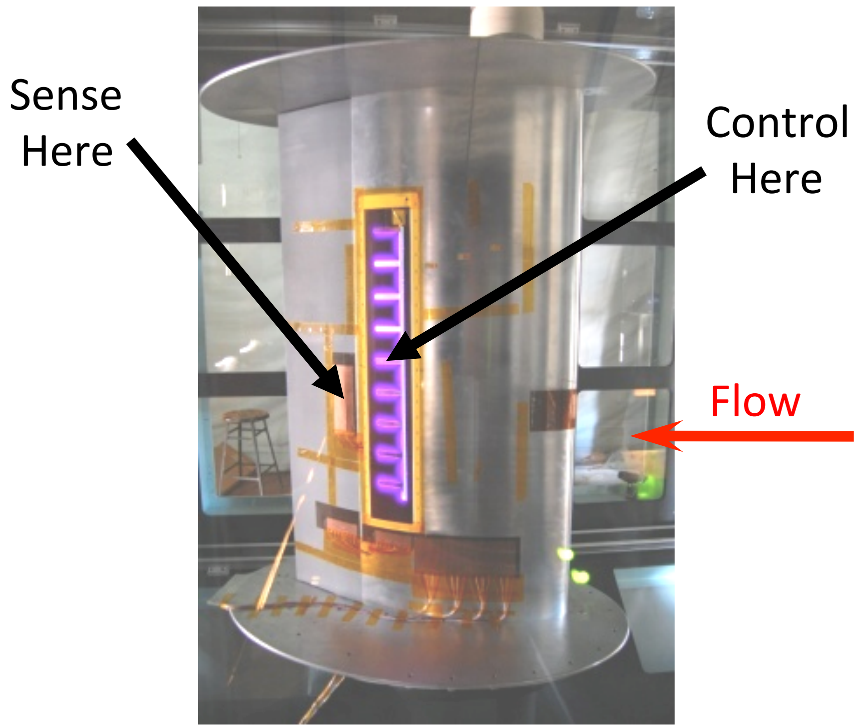

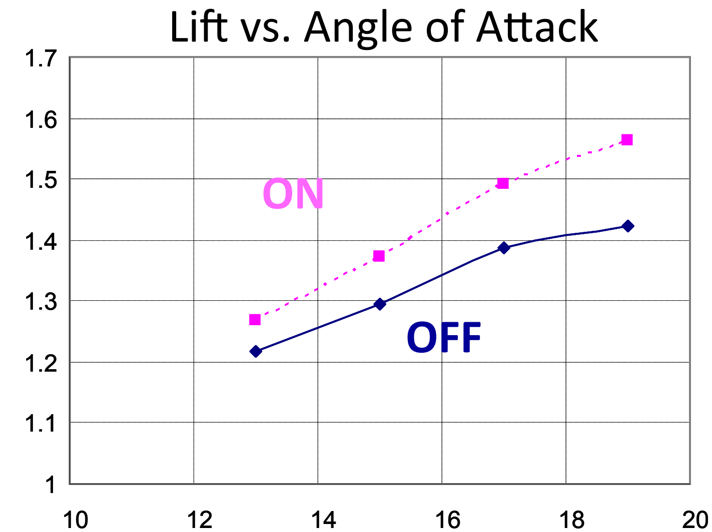

Sweeping 13-17 deg AoA

- Flap hot-film array detects flap separation
- Fixed shear level triggers DBD panel
- Tested in real-time AoA sweeps

Numerical Simulations: Interaction of Actuator and Flow

Specified Electric Body Force
(Semi-Empirical Model)

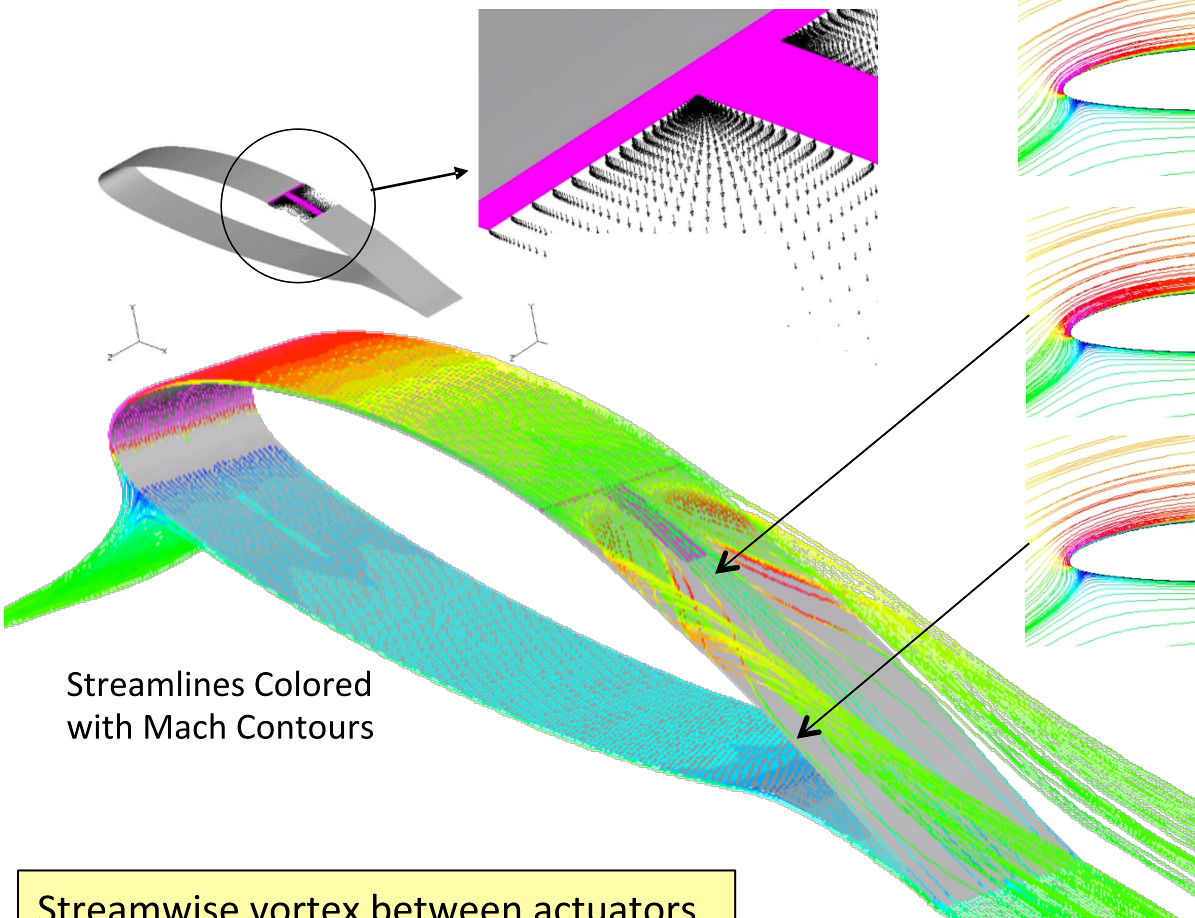

Streamlines Colored with Mach Contours

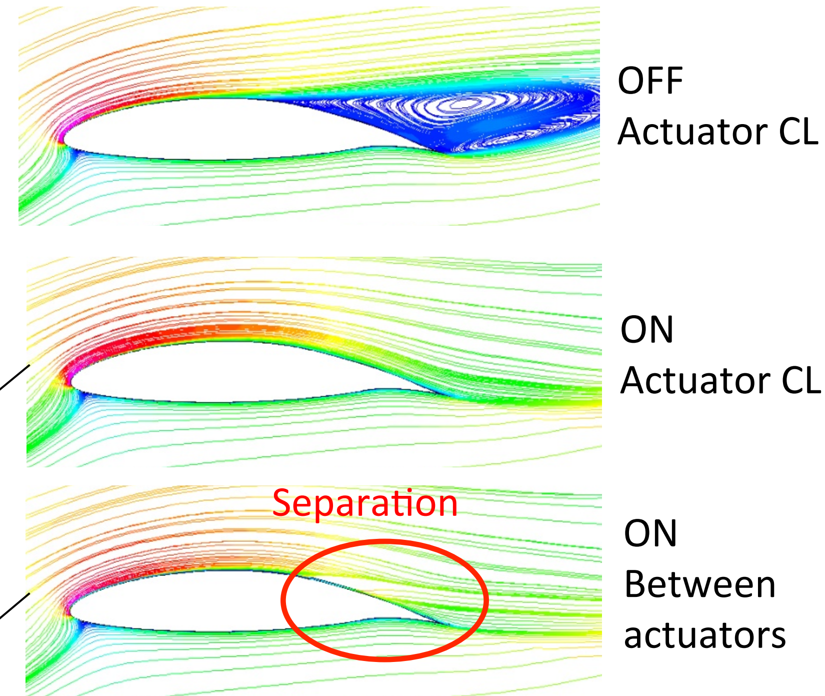

Boeing CFD
3D RANS Computations
Code: BCFD-MHD
Body force: LENPAM

Streamwise vortex between actuators
Separation present between actuators

On to Higher Speeds: Closed-Loop Control with ns-DBD

NACA 0015

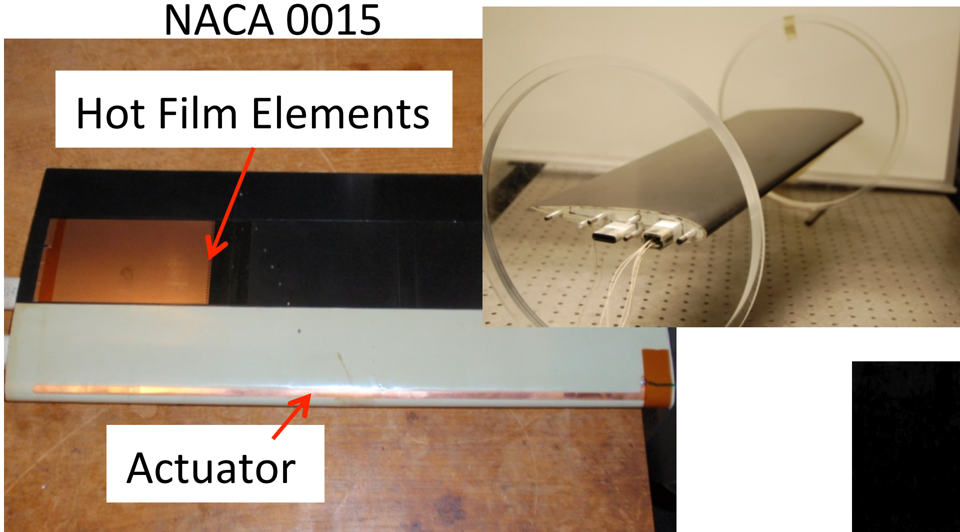

Poggie - *AFRL*
Samimy, Adamovich, Little, et al. - *OSU*
A. Mangalam - *Tao Systems*

AIAA Paper 2011-487

Schlieren Image of Pulse

Control to 93 m/s

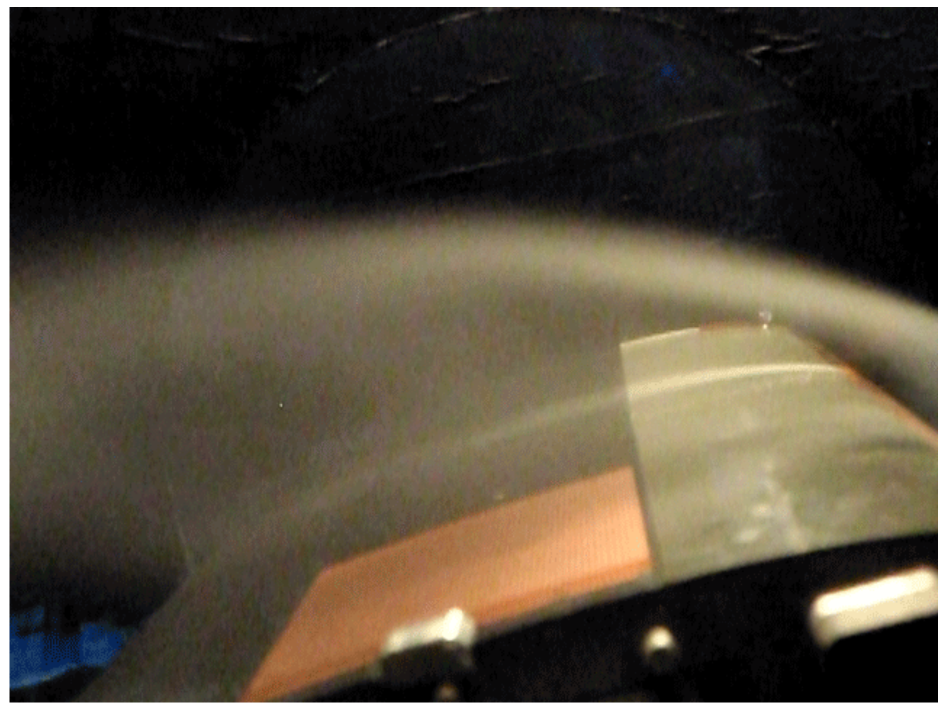

Separation at High Speed: Large-Scale Unsteadiness

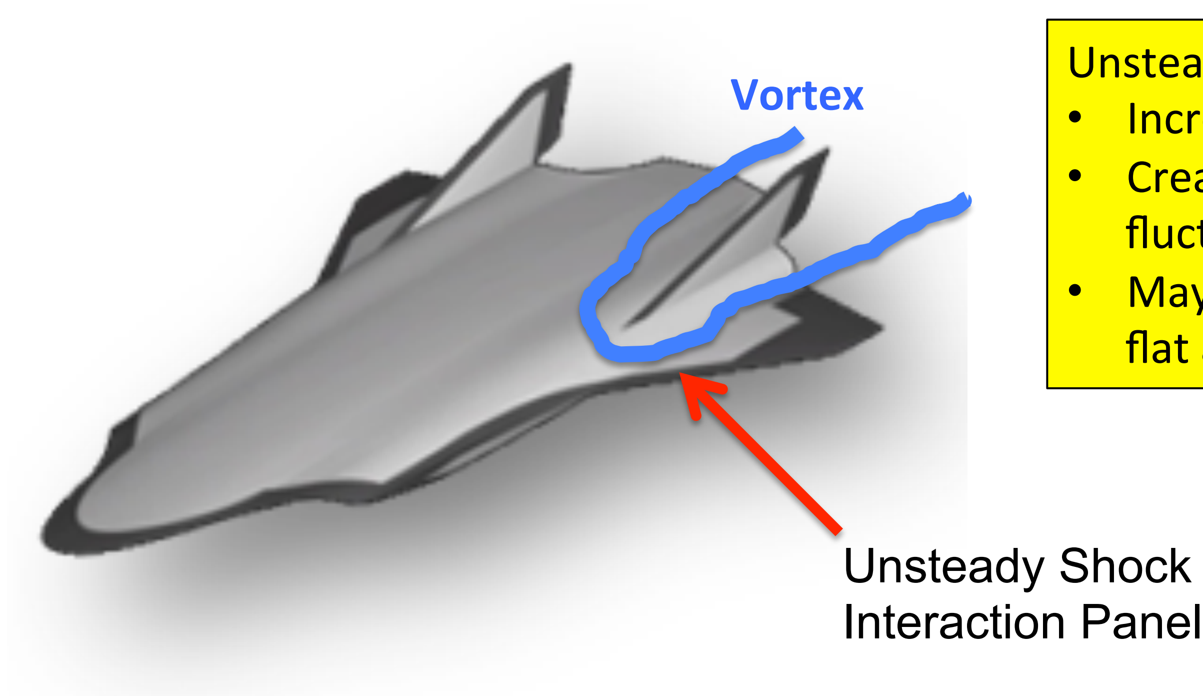

Unsteady separation:
- Increases thermal loads
- Creates intense wall pressure fluctuations
- May drive resonant frequencies of flat aircraft panels

- Fatigue loading from unsteady SWBLI very serious design concern
- Typical for Mach 5 Cruise: 147 dB, 800 K (Zuchowski, AFRL TR, 2012)

Separation Unsteadiness

Amplifier Viewpoint

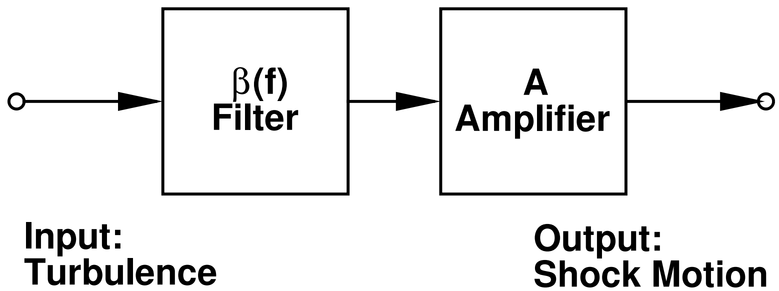

- Plotkin (1975), Ganapathisubramani et al. (2006-2009), Touber and Sandham (2011)
- Low-frequency, large-scale disturbances selectively amplified by separation bubble

Oscillator Viewpoint

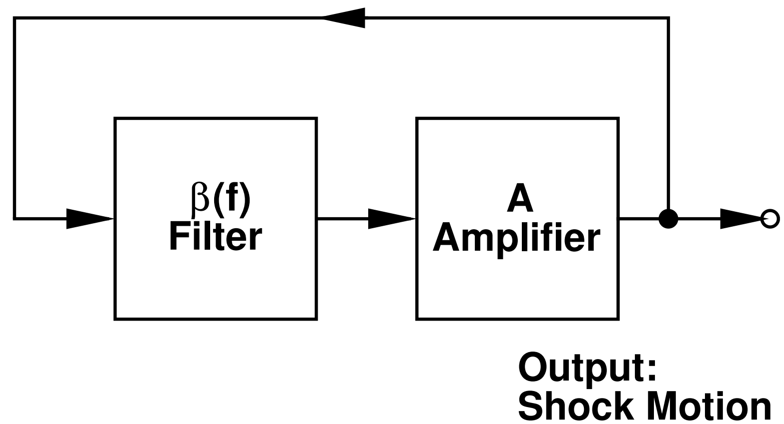

- Trilling (1958), Piponniau et al. (2009)
- Self-excited separation bubble oscillations
- Shear layer instability and entrainment

- These models are not mutually exclusive
- Frequency response depends on separation bubble properties

Plotkin (1975) Model

- Plotkin (AIAA J, 1975)
- Linearly-damped Brownian motion
- Time scales: $\tau_u \ll \tau_R$
- Frequency-selective amplifier
- Cut-off frequency set by separation bubble characteristics
- Input set by TBL

- Model ODE:

$$\dot{x} + x / \tau_R = u(t)$$

- Fluctuation spectrum:

$$\frac{G_p(f)}{\overline{p'^2}\tau_R} = \frac{4}{1 + (2\pi f \tau_R)^2}$$

- Autocorrelation:

$$R_p(t) = \exp(-t / \tau_R)$$

- Fluctuation intensity:

$$\overline{p'^2} = \left(\frac{\partial \overline{p}}{\partial x} \right)^2 \overline{u^2} \tau_u \tau_R$$

Wall Pressure Spectra

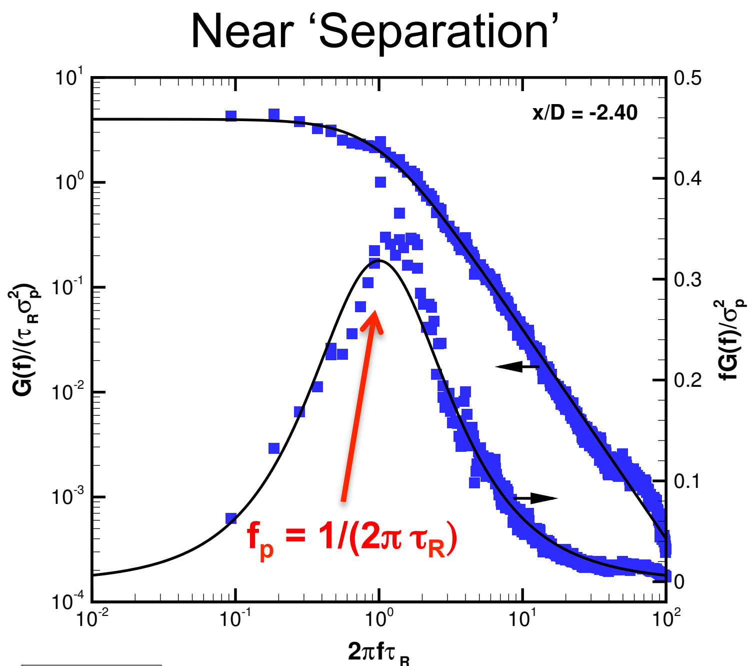

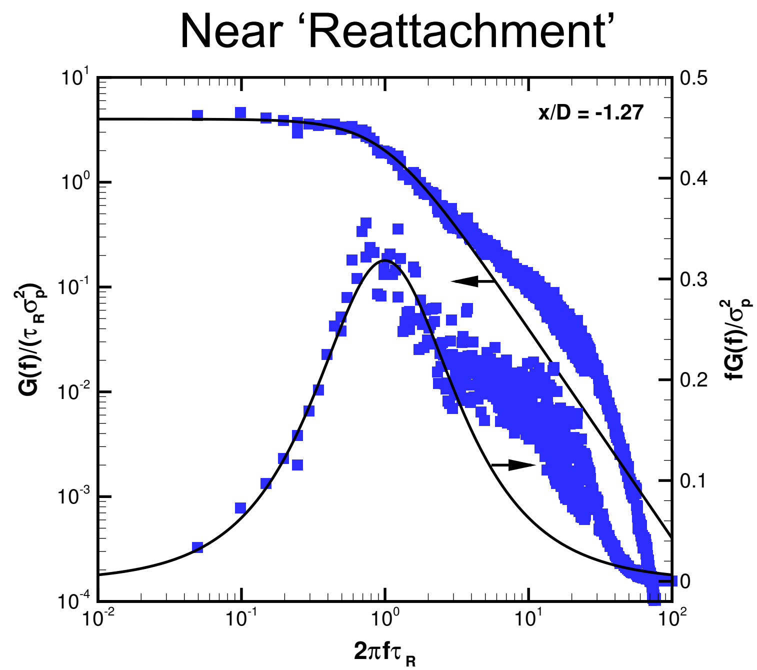

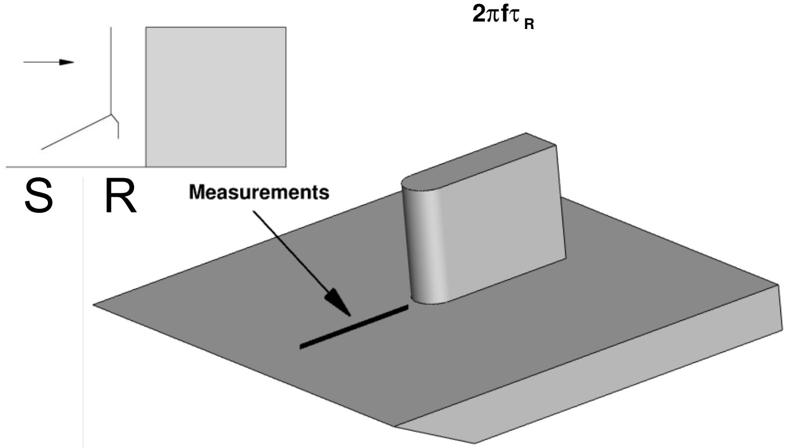

Blunt fin wall pressure spectra (M=3)
Poggie and Smits (2001, 2005)

Wind Tunnel Experiments

Blunt Fin at Mach 5
U. Texas, Austin Group

Wall Pressure Spectra

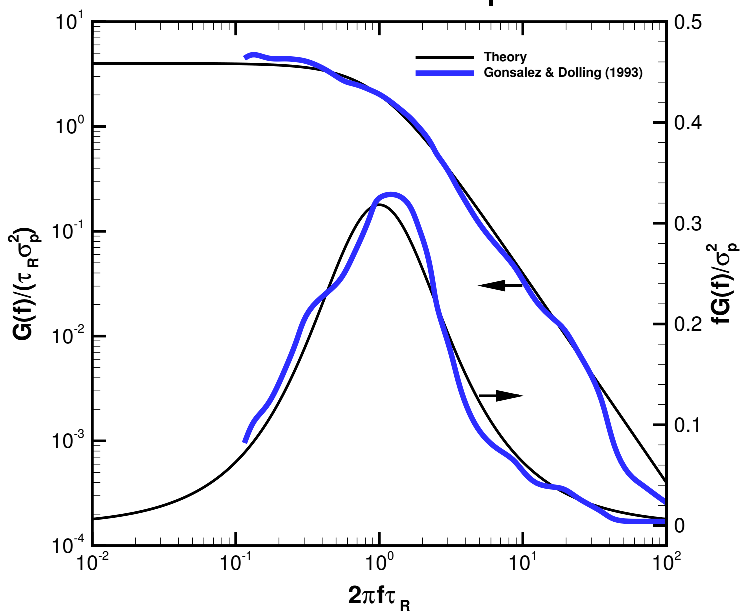

Gonsalez and Dolling (1993)

Shock Position Spectra

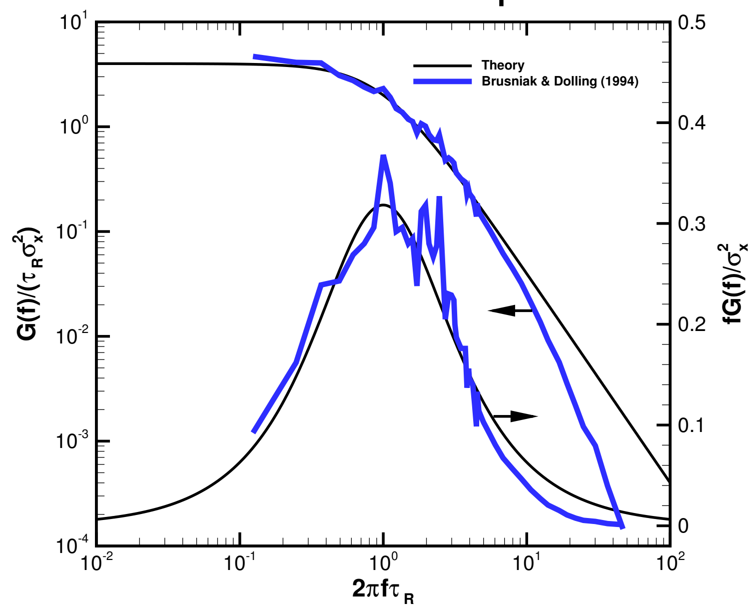

Brusniak and Dolling (1994)

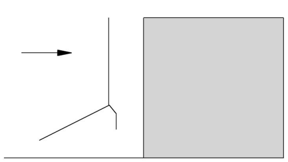

S

- Model fits for different Mach number and tunnel
- Also fits for ***shock position*** spectrum

Flight Test Experiments

HIFiRE-1

Kulite Transducer Stations

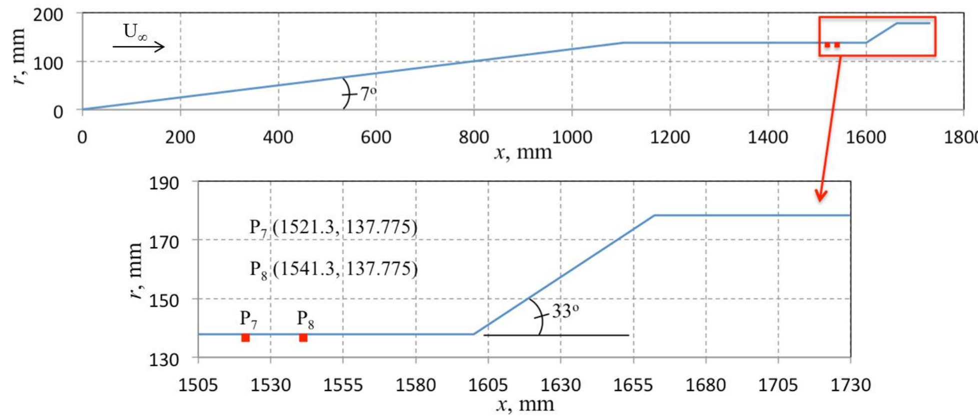

- HIFiRE Flight 1: Woomera Range, March 22, 2010
- Documentation: Stanfield, Kimmel, and Adamczak, AIAA Papers (2012-2013)

Wind Tunnel vs. Flight Test

Pressure Fluctuations
Nondimensional Power Spectral Density

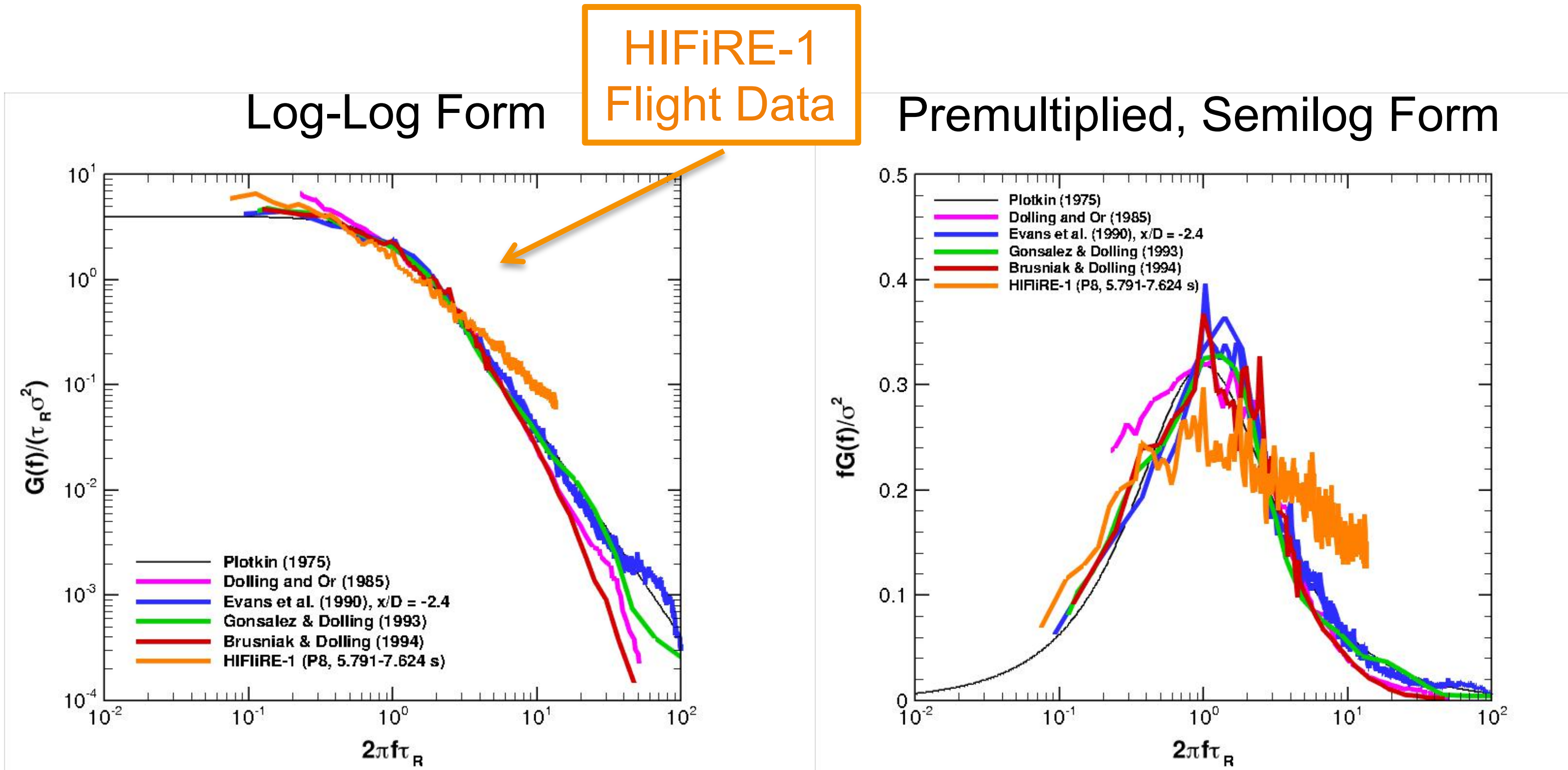

- Relatively good agreement for a variety of ramp and fin configurations, M = 2-5
- Flight data may roll off at a somewhat slower rate
- Motivates examination of pressure transducer frequency response

Large-Eddy Simulation

Compression Ramp Configuration

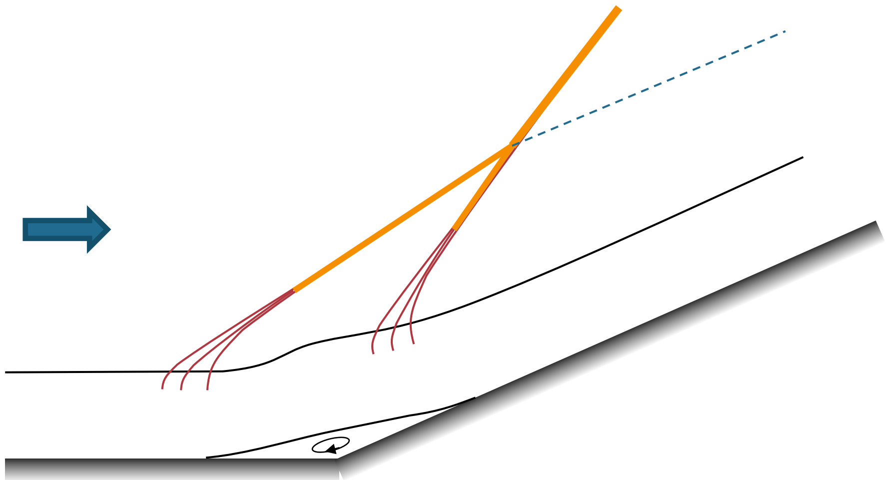

$M = 2.3$, $Re_\theta = 2000$
24 deg ramp

High-Fidelity, Implicit LES
AFRL FDL3DI code
Simulations with 16-188 million cells
Body-force boundary layer trip

Incoming Boundary Layer Profile
van Driest Coordinates

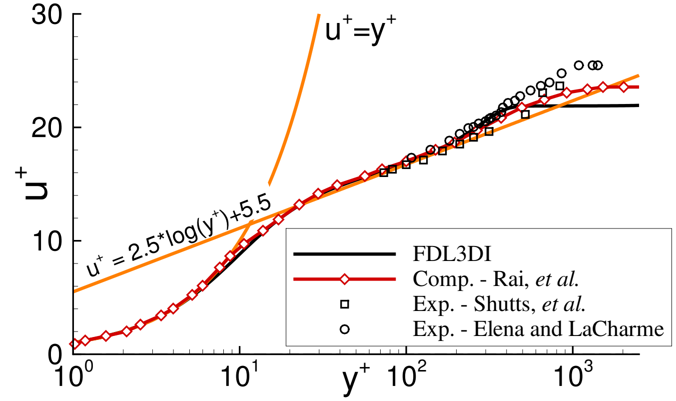

Incoming Boundary Layer
Turbulence Kinetic Energy

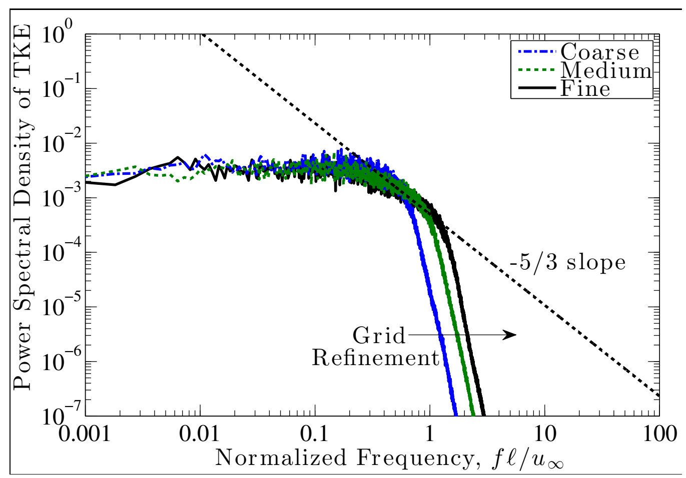

More energy resolved as grid refined

Wall Pressure Statistics

Experimental Results

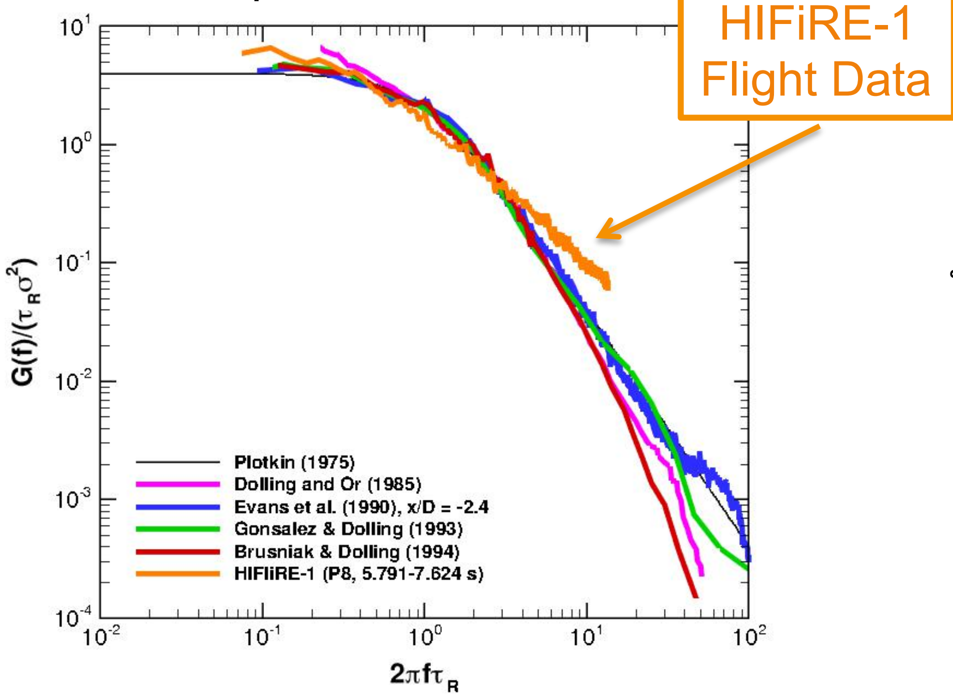

Various configurations, M = 2-5

Computational Results

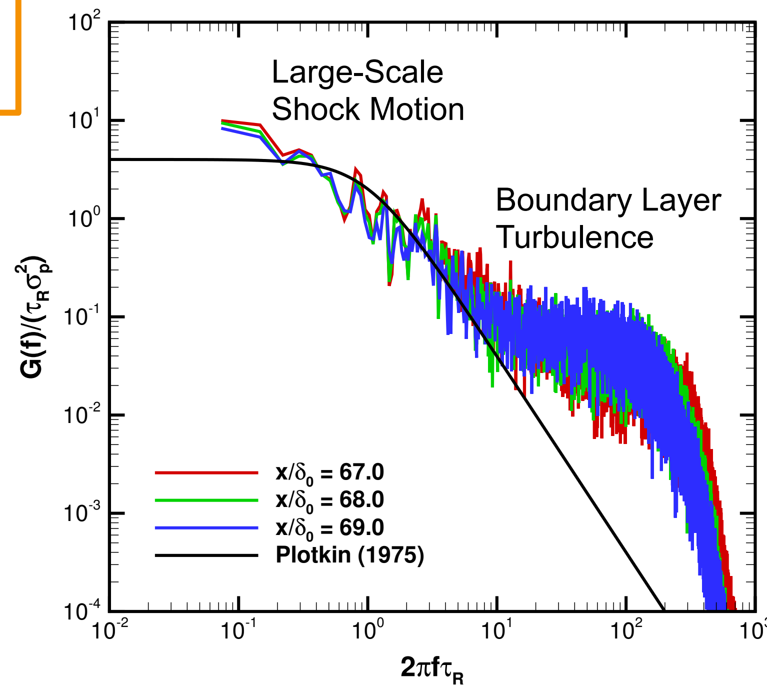

Compression ramp, M = 2.3, 23 deg

Poggie et al., AIAA Journal, 2014

LES captures large-scale unsteadiness

Plasma-Based Control of Unsteady SWBLI

Compression Ramp Configuration

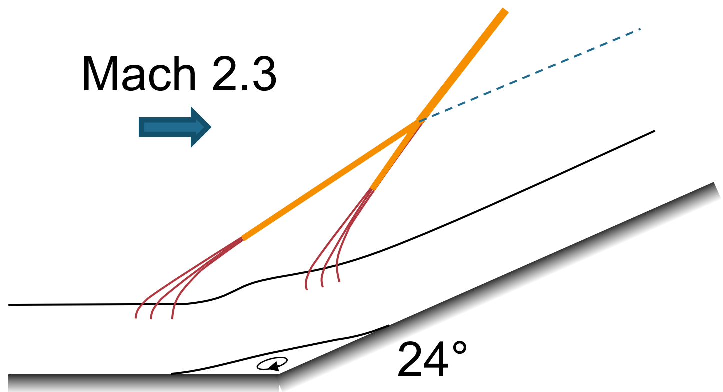

N. J. Bisek, D. P. Rizzetta, and J. Poggie, AIAA Journal, 2013.

Magnetically-Driven Gliding Surface Discharge Actuator

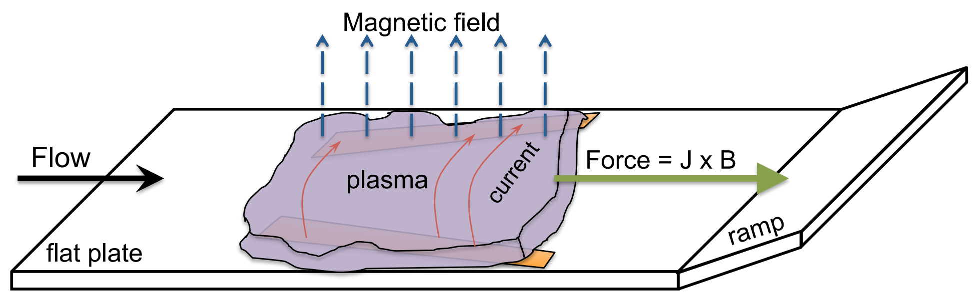

- Explored experimentally by Princeton University group
- Plasma column moves faster than bulk flow
- Imparts momentum and heat
- Reduced order model for LES

Effect of Control

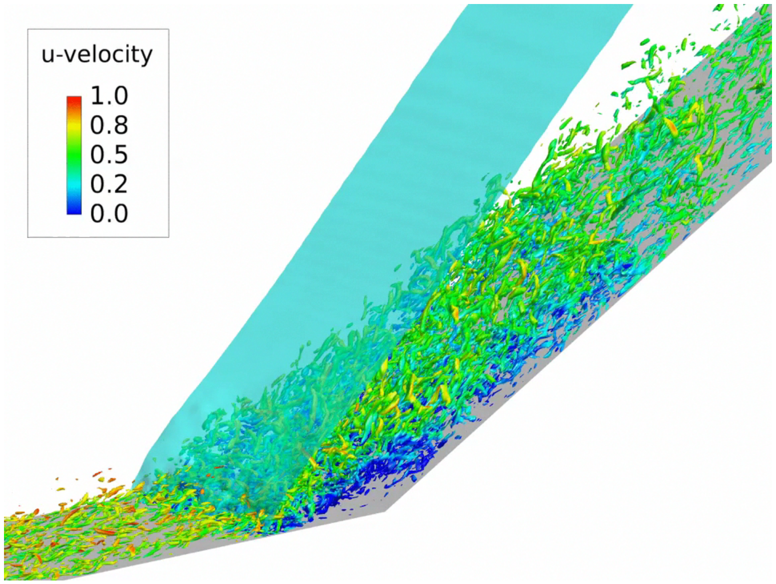

Baseline Case

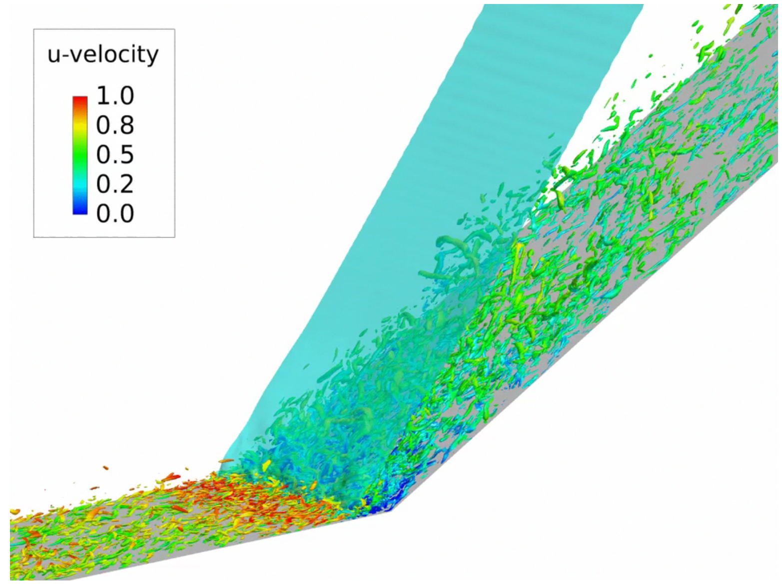

Control Case

PSD of TKE

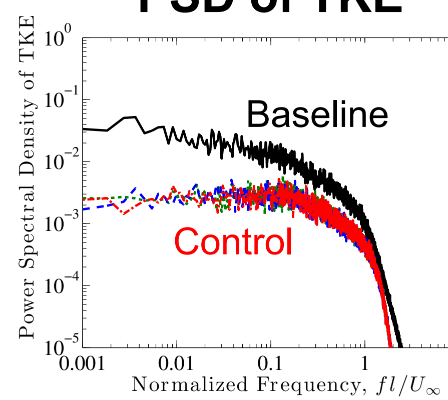

24° Ramp
Mach 2.3
$Re_\theta = 2500$

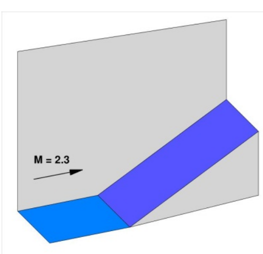

Reduced:

- Size of separation bubble
- Energy in low-frequency wall pressure fluctuations
- Fatigue loading

Turbulent Boundary Layer

Density contours, ρ/ρ_∞

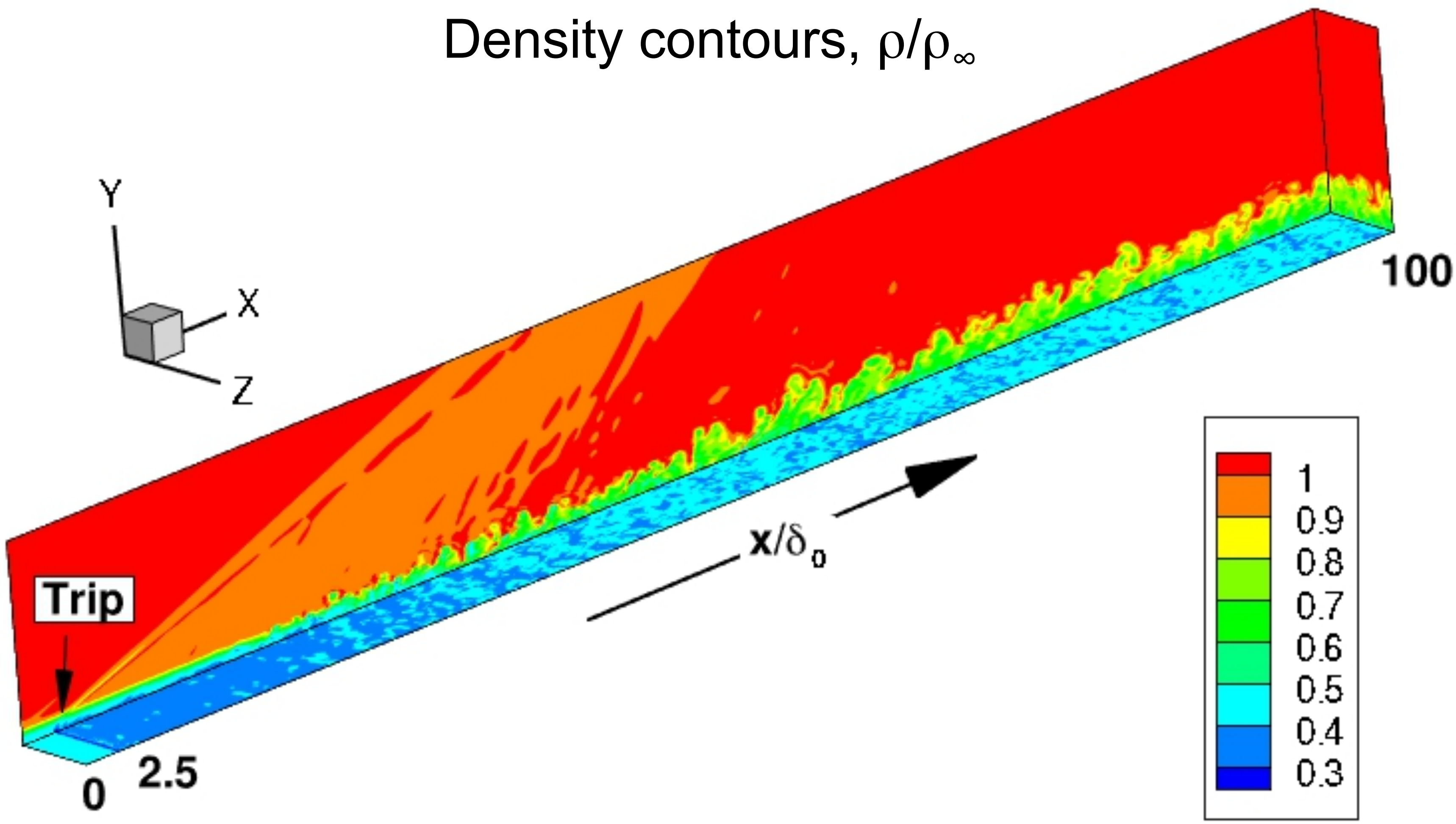

Turbulent Boundary Layer: Comparison to Experiment

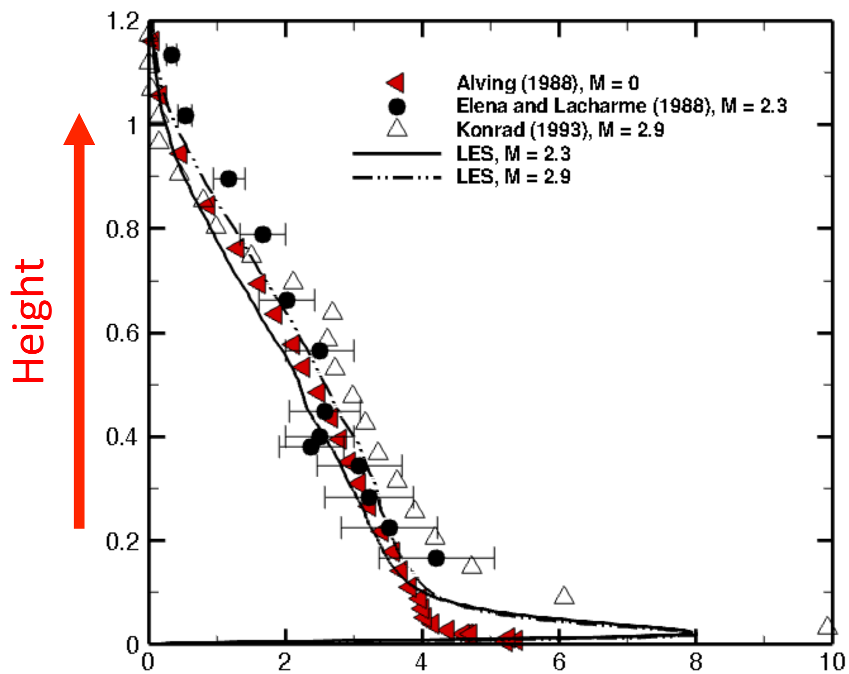

Velocity Fluctuations

Side View: Density Contours

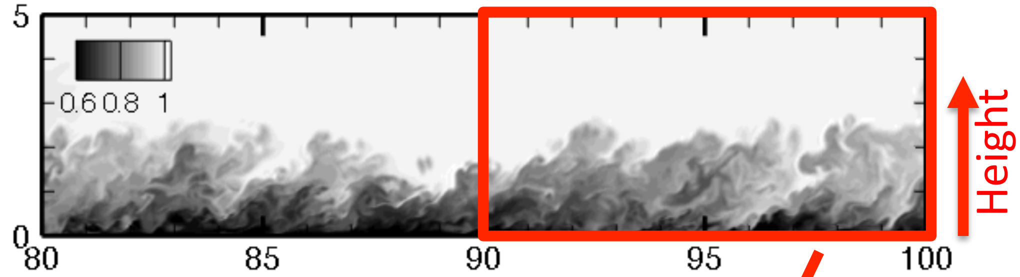

M = 2.3, $Re_{\theta i}$ = 2000

Laser Scattering Experiments
M = 2.9, $Re_{\theta i}$ = 36000
Poggie et al., Experiments in Fluids, 2004

Turbulent Boundary Layer

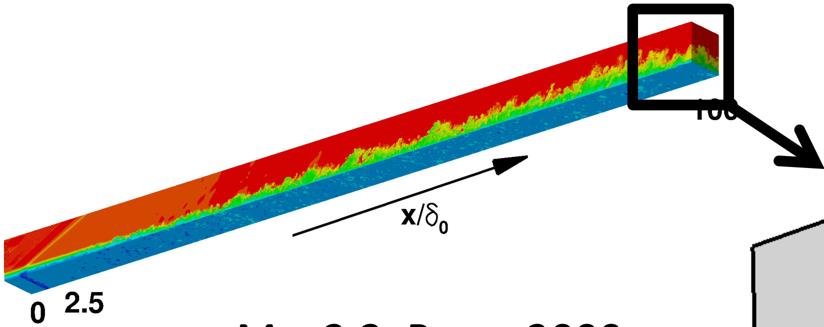

M = 2.3, $Re_{\theta i}$ = 2000

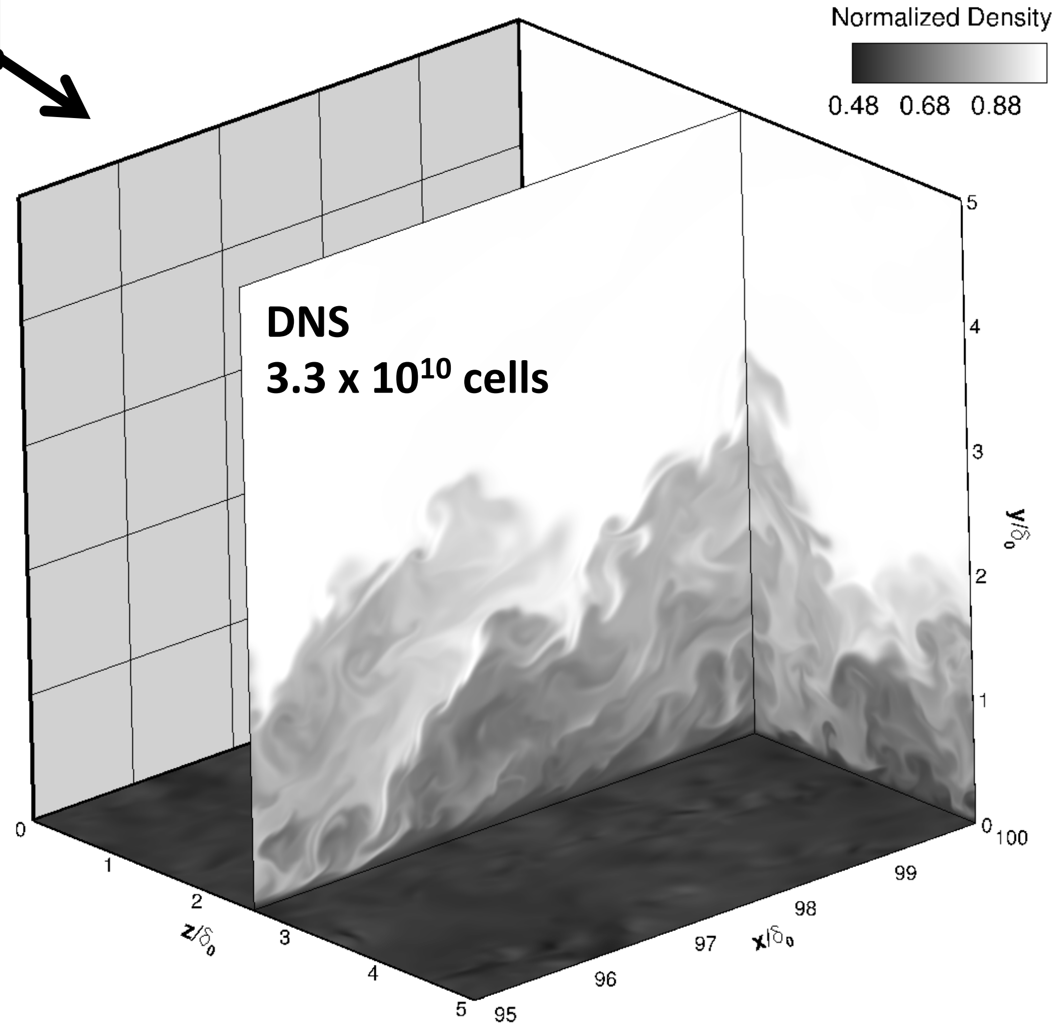

Turbulent Boundary Layer: Effect of Resolution

Density Field – End View Looking Downstream

Large Eddy Simulation (LES)

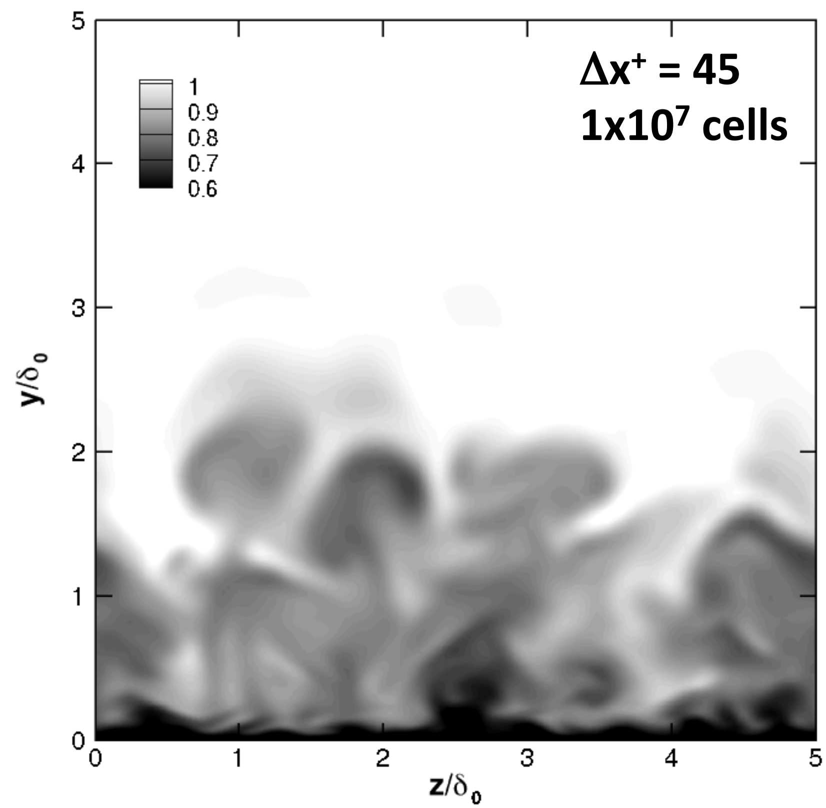

Direct Numerical Simulation (DNS)

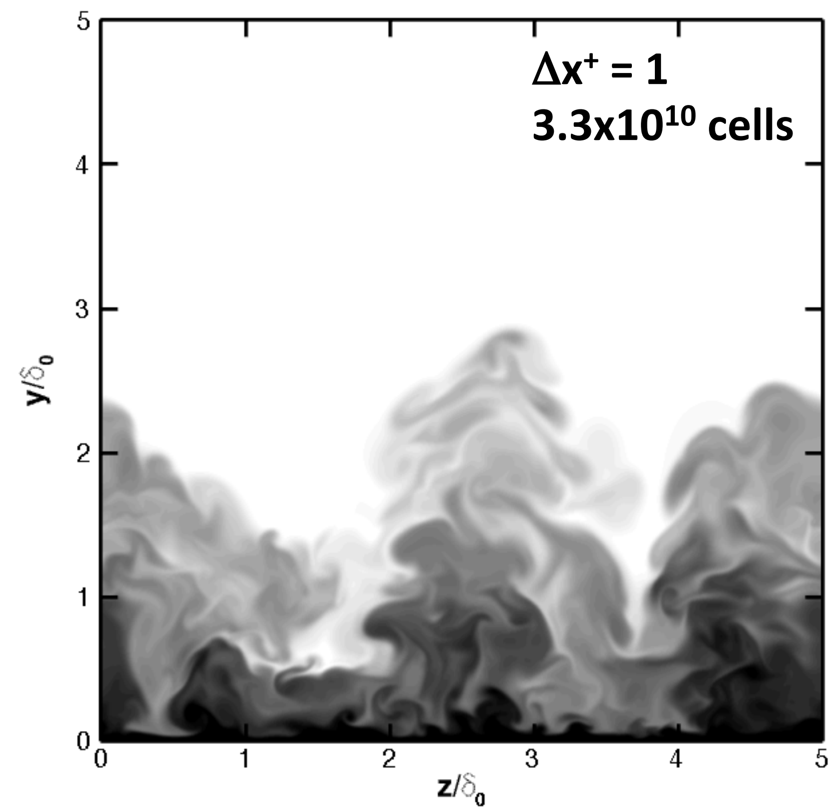

LES is an approximation

High-Frequency Content: Effect of Resolution

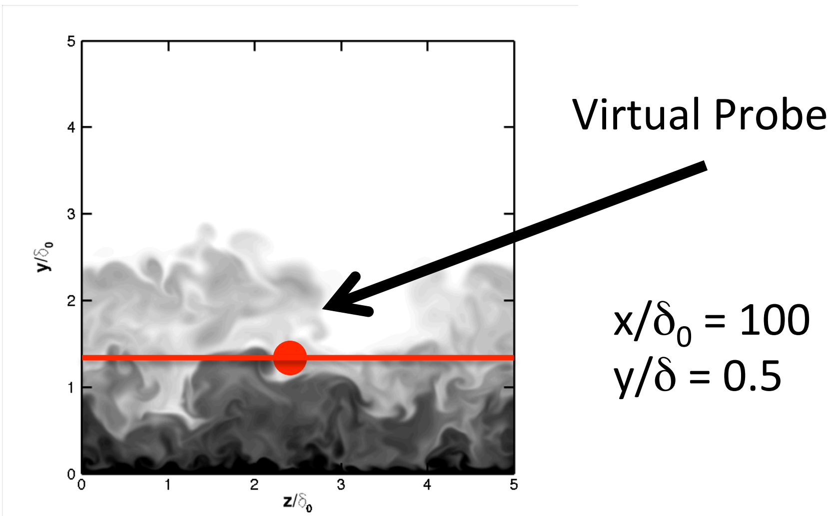

Spectral convergence indicates full resolution

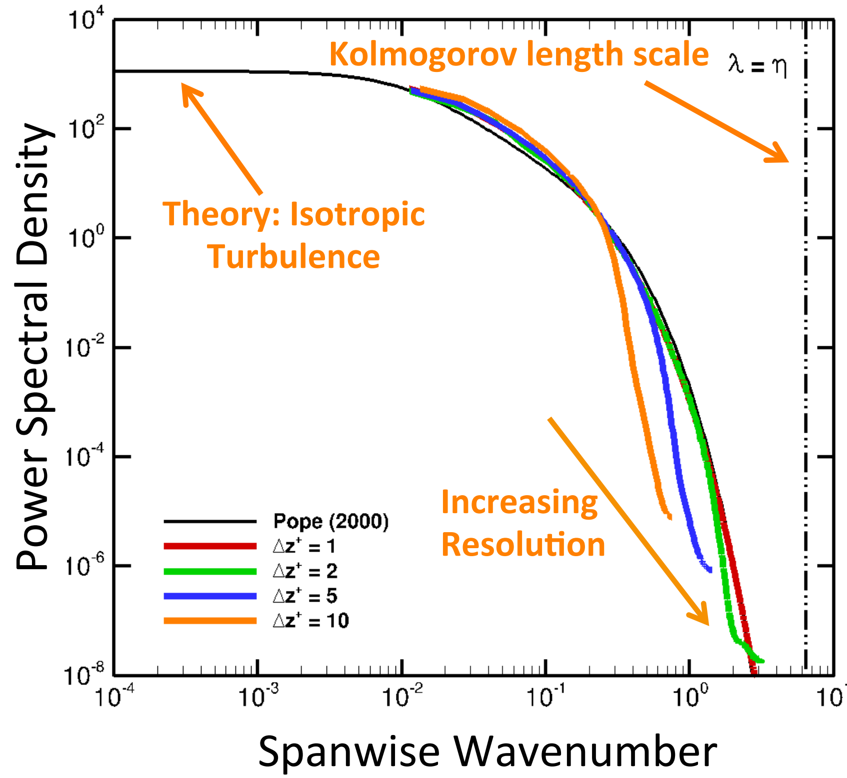

Low-Frequency Content: Effect of Domain Width

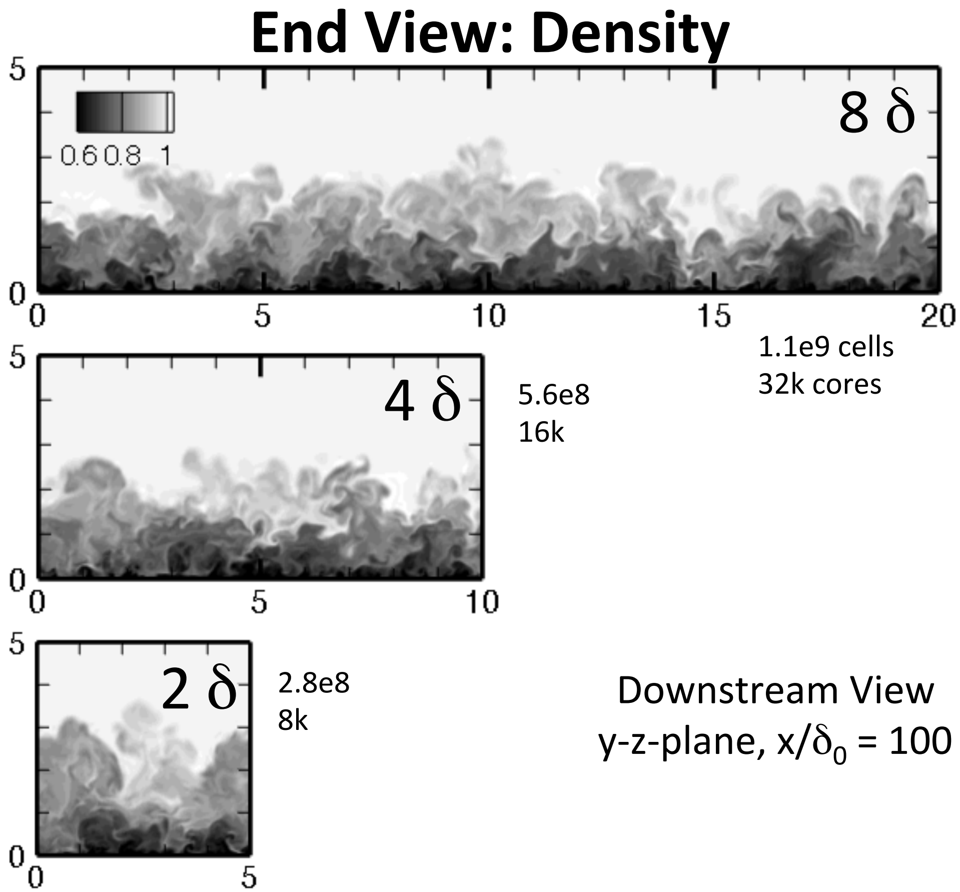

Downstream View
y-z-plane, $x/\delta_0 = 100$

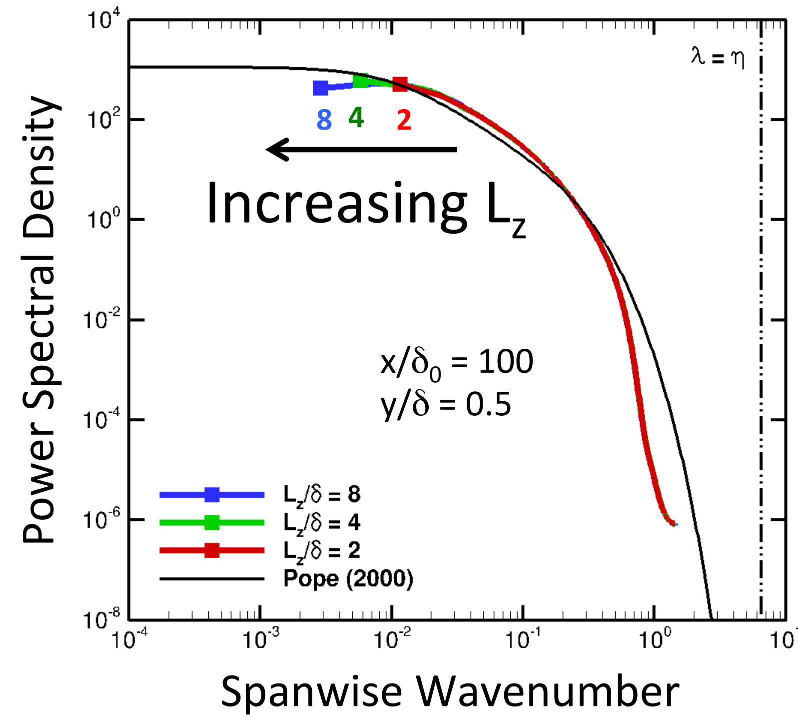

Low frequencies drive separation unsteadiness and structural loading

Summary and Conclusions

- Plasma aerodynamics has a long history, and an exciting future
- Necessary to understand both fluid mechanics and actuator physics
- Large computations compare well to experiment; draw together physics of plasmas and fluids